DOT/FAA/TC-20/31

Federal Aviation Administration
William J. Hughes Technical Center
Aviation Research Division
Atlantic City International Airport
New Jersey 08405

Lithium Battery Cell Separator Dendrite Detection

06/29/2020

Final report

U.S. Department of Transportation
Federal Aviation Administration

NOTICE

This report is available at the Federal Aviation Administration William J. Hughes Technical Center's Full-Text Technical Reports page: actlibrary.tc.faa.gov in Adobe Acrobat portable document format (PDF).

Form DOT F 1700.7 (8-72) Reproduction of completed page authorized

1. Report No.	2. Government Accession No.	3. Recipient's Catalog No.
DOT/FAA/TC-20/31		

4. Title and Subtitle	5. Report Date
Lithium Battery Cell Separator Dendrite Detection	06/29/2020
	6. Performing Organization Code

7. Author(s)	8. Performing Organization Report No.
Dr. Jitendra Kumar	

9. Performing Organization Name and Address	10. Work Unit No. (TRAIS)
University of Dayton Research Institute (UDRI) Power and Energy Division Solid-State Battery & Integrated Systems Laboratory 300 College Park, Dayton, OH 45469-0170	11. Contract or Grant No. DTFACT-16-C-00045

12. Sponsoring Agency Name and Address	13. Type of Report and Period Covered
US. D.O.T./Federal Aviation Administration William J. Hughes Technical Center ANG-E271 Atlantic City International Airport, NJ 08405 Phone: 609-485-8493	14. Sponsoring Agency Code AAQ610-AFN

15. Supplementary Notes

The Federal Aviation Administration William J. Hughes Technical Center Aviation Research Division COR was Michael Walz.

16. Abstract

To address the well-known thermal runaway (battery fire) nature of commercial lithium ion (Li-ion) batteries, the University of Dayton Research Institute (UDRI), in partnership with its subcontractor, UES Inc., is developing and testing technology that fundamentally addresses the causes of thermal runaway in Li-Ion batteries. This includes the development of a thermally stable and dendrite growth-limiting separator, and an early dendrite sensing mechanism built into a battery separator.

In this 3-year program, UES fabricated different solid-state ceramic electrolyte thin-films on commercial separators and UDRI tested those ceramic-coated separators for their thermal stability, safety improvement (shut-down, break-down) and electrochemical performances. Moreover, UDRI developed an early dendrite sensing layer on the separator that when tested in real working Li-ion cells, has shown a 25 sec time lag before dendrite detection and actual cell shorting. This 25 sec time lag between dendrite sensing and cell shorting can be enough to trigger battery shutdown signal of a battery management system, which would prevent thermal runaway/battery short circuit events. This discovery was supported by a significant volume of carefully planned and reproducible data, which is outlined in this report. The developed thermally stable separator with built-in dendrite formation resistance and sensing technology does need further investment and testing before it can be transitioned to commercial large format (Ah level) Li-Ion batteries and battery packs.

17. Key Words	18. Distribution Statement
Battery separator, thermal stability, safety, dendrite detection, electrochemical performance.	This document is available to the U.S. public through the National Technical Information Service (NTIS), Springfield, Virginia 22161. This document is also available from the Federal Aviation Administration William J. Hughes Technical Center at actlibrary.tc.faa.gov.

19. Security Classif. (of this report)	20. Security Classif. (of this page)	21. No. of Pages	22. Price
Unclassified	Unclassified	63	

ACKNOWLEDGEMENTS

The financial support from the Federal Aviation Administration (FAA) under contract # DTFACT-16-C-00045 is greatly appreciated. The principal investigator (PI) and team sincerely thank Mr. Michael Walz (FAA), the technical monitor of this project for his support and feedback on the progress throughout the project duration. Sincere thanks to Ms. Keren Mercer (FAA), the contract facilitator for her timely support. PI greatly acknowledges the contribution of UDRI battery team members (Dr. Priyanka Bhattacharya, Dr. Badri Shyam, Dr. Yuxing Wang, Dr. Alexander B. Morgan, Dr. Guru Subramanyam, Mr. Robert Kauffman, Mr. Nicholas Valo (Ph.D. student), Mr. Ashish Gogia (Ph.D. student), and UDRI support staff) and subcontractor at UES Inc. (Dr. A.K. Rai and Dr. Rabi Bhattacharya).

Contents

Figures

Tables

Acronyms

Acronym	Definition
BMS	Battery Management System
DMC	Dimethyl Carbonate
EB-PVD	Electron Beam-Physical Vapor Deposition
EC	Ethylene Carbonate
EIS	Electrochemical Impedance Spectroscopy
EMC	Ethyl Methyl Carbonate
FAA	Federal Aviation Administration
LAGP	Lithium Aluminum Germanium Phosphate
LIB	Lithium Ion Battery
LiSICON	Lithium Superionic Conductor
LLZO	Lithium Lanthanum Zirconium Oxide
LSPS	Lithium Tin Phosphorus Sulfide
NMC	Nickel Manganese Cobalt Oxide
PE	Polyethylene
PI	Polyimide
PP	Polypropylene
PVDF	Polyvinylidene fluoride
SEM	Scanning Electron Microscopy
TMS	Battery Thermal Management
UDRI	University of Dayton Research Institute
VC	Vinylene Carbonate
XRD	X-ray Diffraction

Executive summary

To address the well-known thermal runaway (battery fire) nature of commercial lithium ion (Li-ion) batteries used in aircraft, the University of Dayton Research Institute (UDRI), in partnership with its subcontractor, UES Inc., developed and tested thermally stable and dendrite resistive separators. UDRI also developed and tested an early dendrite sensing technique built into this battery separator that can minimize the risk of thermal runaway events in Li-ion. By focusing on this technology, the underlying causes of thermal runaway in Li-ion batteries could be addressed, thus inherently improving the fire safety of these batteries in aircraft, regardless of battery location and size.

In this program, UDRI implemented and tested different solid-state ceramic electrolyte thin-film coated separators prepared by UES Inc. for their improved thermal stability and tested metal/ceramic-coated separators for dendrite sensing capability. The main results achieved are as follows:

- Separators with improved thermal stability: UDRI's patented high temperature (stable >1000°C in air) solid ceramic electrolyte material and ceramic electrolytes obtained from commercial vendors were used to coat binder-free, thin-film thermal and dendrite barrier layers (20 nm-500 nm thick) on both sides of polymer separators using different physical evaporation techniques. These new separators, which should not melt and fail beyond 200°C in an unexpected thermal heating during storage or operation and thermal heating due to cell short circuit, were compared with commercially available separators to confirm that they did provide superior thermal protection, and still met battery performance requirements.
  - UDRI's ceramic electrolyte, when coated on commercially used separator, was observed to demonstrate a significant delay in thermal shrinkage, thermal rupture, separator shutdown, and separator breakdown vs. uncoated separators. This improvement will delay and minimize Li-ion battery thermal runaway. Furthermore, the ceramic coating either improves the base battery electrochemical performances of Li-ion or, at minimum, preserves the electrochemical performances compared to best Li-ion separator available in today's market, depending upon which underlying separator technology is used.

- Separator with early dendrite detection capability: The critical finding of the project was a demonstration of an early dendrite sensing layer on a thermally stable separator that, when tested in working Li-ion cells, has shown a 25-second time lag between dendrite detection and actual cell shorting. This 25-second time lag between dendrite sensing prior

to cell shorting can be enough to trigger a battery shutdown signal of a battery management system (BMS), which would be highly likely to prevent a thermal runaway event from even happening. This technology does require more testing and development to advance it for robust use in commercial Li-ion cells and/or future format cells.

The discoveries in this funded effort were successful in addressing two of the underlying fundamental causes of Li-ion battery thermal runaway events, namely melting/rupturing of battery separators, and dendrite propagation. By preventing separator rupturing and dendrite formation, the underlying causes of battery fires are addressed and thus no heavy enclosures to capture battery fires would be required on aircraft. Further, addressing this underlying cause greatly improves electrical storage on aircraft for current and future aviation systems. With further technology development, the two advances in this funded effort can likely be transitioned to improve Li-ion battery safety for aircraft.

1 Introduction

Lithium-ion (Li-ion) batteries contain thermally unstable cell components (electrodes, electrolyte, separator) that can create a potentially hazardous event (battery fire) when exposed to conditions such as crush, over-charge, over-discharge, high temperature, and internal short circuit. This is exemplified by the recent grounding of Boeing 787 commercial airliners brought about by Li-Ion battery failures. In the event of cell failure and rise in temperature, the battery separator can melt or fracture (around 100-150°C) leading to direct electrical contact between electrodes (electrical shorts). Electrical shorts allow a huge current flow between electrodes that produces heat. The heat generated during an electrical short of a cell causes a sudden increase in the internal cell temperature that triggers decomposition of the interior battery components (see Figure 1). This rapid exothermic event, which often results in the decomposed battery components igniting and burning, produces a huge amount of heat that is beyond the capability of natural cooling or even the cooling that can be provided by battery thermal management (TMS), and hence the phrase “thermal runaway” is used when this occurs in a Li-ion battery (Figure 1) [1]. Thus, to prevent thermal runaway, first and foremost, the separator must be made thermally stable, at least up to a temperature >200°C, so that decomposition of electrolyte, cathode, and anode can be either delayed or completely avoided [2].

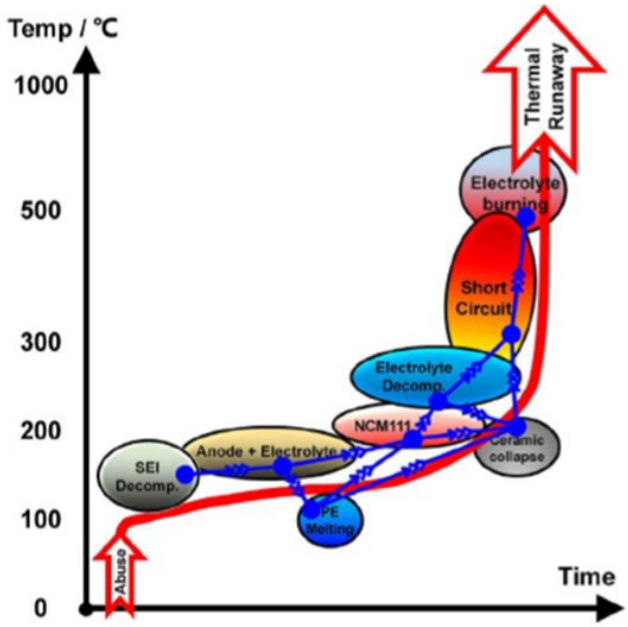

Figure 1. Battery thermal runaway process

The current commercial approach to improve the thermal stability of the battery separator typically involves slurry coating of thermally stable ceramic materials (thickness, ~2 μm) on both sides of the separator [3]. However, the commercial ceramic-coated separators can still melt or fracture above 160°C, because the binder used in coating this slurry dissolves in liquid electrolyte of a Li-ion battery above 80°C, leaving ceramic particles loose from the separator surface. Furthermore, the ceramic layers in commercial separator are porous (which may allow growth of dendrite) and thick (which will negate battery energy density) and hence not ideal. To further improve the thermal stability of the commercial separator and overall Li-ion cell performances, a thin, dense (a pore free ceramic layer can be ideal), and binder-free ceramic coating must be developed [4].

During this FAA-funded project (DTFACT-16-C-00045), UDRI has developed such a *thin (20-500 nm), nearly dense, and binder-free* ceramic coating using physical vapor deposition techniques that make UDRI's ceramic-coated separators thermal stable (does not melt or fracture beyond 200°C).

Though UDRI's thin-film ceramic-coated separator improves thermal stability beyond 200°C and delays dendrite growth, there still can be danger of dendrite growth as the ceramic layer is not 100% dense up to a 500 nm ceramic layer. A ceramic layer more than 500 nm can be completely dense, but may negatively impact cell cycling performance. Therefore, in addition to UDRI's ceramic-coated separator with optimal ceramic layer thickness and densification, a method that can provide early cell shorting warning before actual cell shorting might be useful [5] in developing a thermal fail-proof Li-ion battery. This would allow the 500 nm ceramic layer to provide practical thermal protection of the separator, and the early dendrite detection system to serve as the "backup" protection technology for the entire Li-ion battery. During this project, UDRI has developed such a dendrite detection technique that provides at least a 25-second early dendrite growth warning, which can be a valuable time period for a battery management system (BMS) to observe the signal from detection, stop battery operation, and avert thermal runaway.

2 Technical progress

2.1 Thin-film ceramics-coated separator and preliminary testing

The thin-film, binder-free, ceramic-coated separator generated by UDRI relied on a three-layer system, as shown in Figure 2 [4]. In this design, a 12 μm, flexible, commercial porous separator (obtained from Entek, http://entek.com/lithium-ion/) is used as a substrate to deposit ceramic layers on both sides of it, using different physical vapor deposition techniques such as Electron

Beam Physical Vapor Deposition (EB-PVD) and Sputtering. Ceramic material can be active (Li^+ conducting, example phosphate glass ceramics e.g. $Li_{1+x}Al_xGe_{2-x}(PO_4)_3$, (LAGP)) [6], garnet-type metal-oxide ceramics e.g. $Li_{6.4}La_3Zr_{1.4}Ta_{0.6}O_{12}$, (LLZ)) [7], and sulfides ($Li_{10}GeP_2S_{12}$ (LGPS) or $Li_{10}SnP_2S_{12}$ (LSPS)) [8], or inactive (insulating ceramics, example Al_2O_3) [9]. The advantage of using active ceramic coating is to assist in Li^+ conduction desirable for better electrochemical performance, in addition to thermal stability. Since EB-PVD and Sputtering leaves all the deposited ceramic layers amorphous, ceramics need to recrystallize to achieve original Li^+ conductivity after deposition. The crystallization temperatures depend on the type of ceramic electrolytes used, but are generally several hundred degrees Celsius beyond the melting temperature of most of the commercial separators available. Therefore, to achieve the full potential of active ceramic coating and achieve both thermal and electrochemical performance in a single system, several options will have to be investigated, including the use of high temperature separator, short crystallization time, or low thickness of ceramic layers. Several active and inactive ceramics, their different thicknesses, different separators (low to high melting), and crystallization temperatures have been investigated for this purpose.

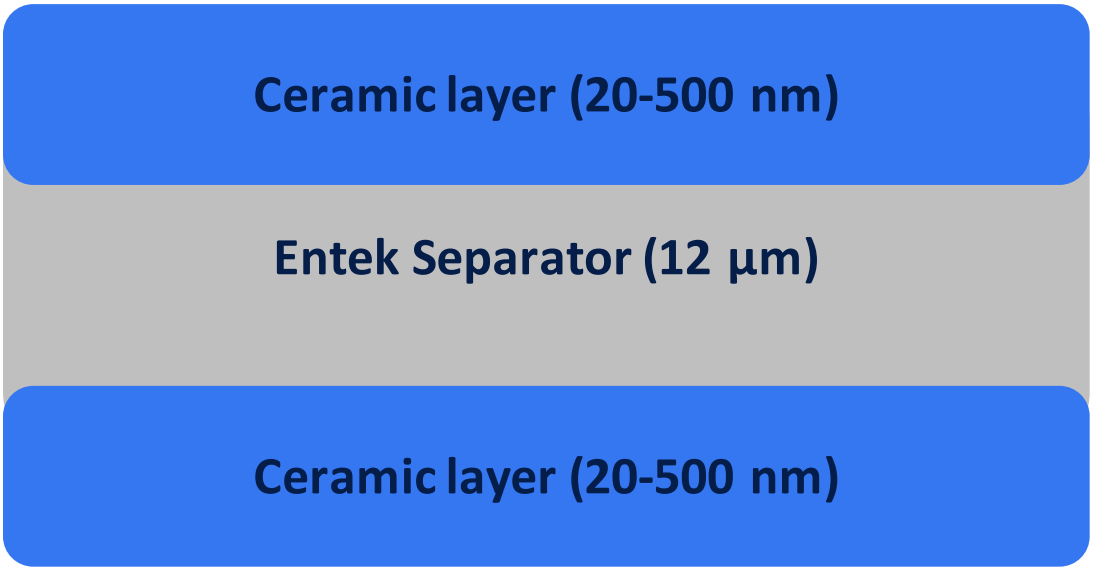

Figure 2. Thin-film ceramic-coated separator design

2.1.1 UDRI's ceramic electrolyte on Entek separator

Initial studies on ceramic-coated separator development focused on the use of UDRI's active ceramic lithium aluminum germanium phosphate (LAGP) [4, 6] material for coating thickness

20 nm to 500 nm and their characterizations, including surface morphology, thermal stability, adhesion to separator, liquid electrolyte wettability, safety (separator shutdown and breakdown) behavior, electrical, and Li-ion cell cycling performances. LAGP was deposited on both sides of the Entek separator using two different techniques, EB-PVD and magnetron sputtering. Figure 3 shows:

i) morphology of separator before ceramic coating (Figure 3a)
ii) 20 nm and 100 nm LAGP coating on separator using EB-PVD technique (Figure 3b and 3c)
iii) 20 nm and 100 nm LAGP coating on separator using sputtering technique (Figure 3d and 3e).

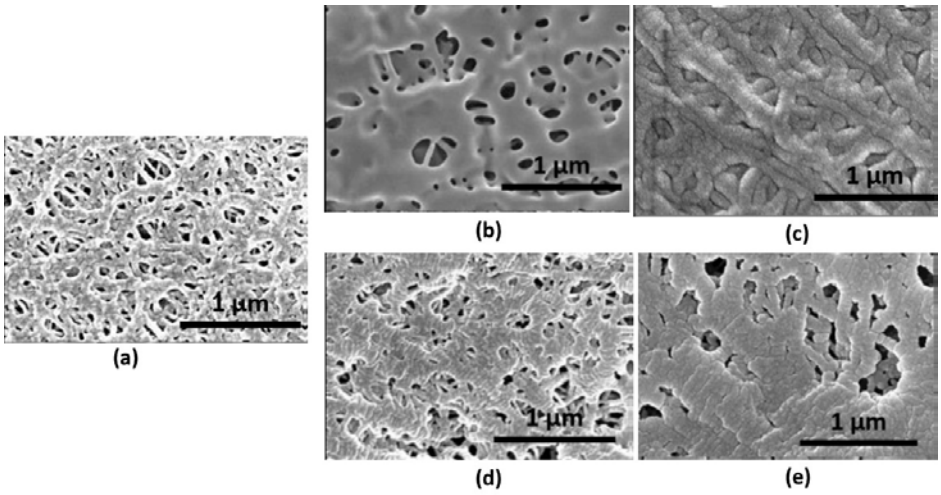

Figure 3. Surface morphology of LAGP-coated Entek separators

With both EB-PVD and sputtering (Figure 3), the separator surface covering by ceramic (LAGP) increases with an increase in the thickness of the deposited ceramic layer. EB-PVD coats the separator along the surface (line of sight coating) and hence covers the separator surface faster (with lesser thickness of ceramic) compared to sputtering, which coats the separator around its fibers (conformal coating) and hence requires a thicker coating to cover pores of separators. As LAGP is a high temperature and Li^+ conducting material, the uniformity and thickness of the ceramic layer on the separator will determine the thermal stability and electrochemical performances of the Li-ion battery using these separators.

Figure 4 shows the thermal stability (percentage shrinkage) of pristine polyethylene (PE) from Entek, 100 nm LAGP-PE-LAGP (sputtering), and 100 nm LAGP-PE-LAGP (EB-PVD)

separators up to 200°C for 2 hours in air. Clearly, LAGP when coated on PE separator using EB-PVD technique shows the highest thermal stability. LAGP-coated PE (EB-PVD) shrinks only 10% when kept at 200°C for 2 hours, whereas sputtering coated separator shrinks by 45% and non-coated PE shrinks by 70% of their original sizes. From Figure 3 and Figure 4, LAGP coating from EB-PVD provides better coverage of separator surface and significantly improves the thermal stability.

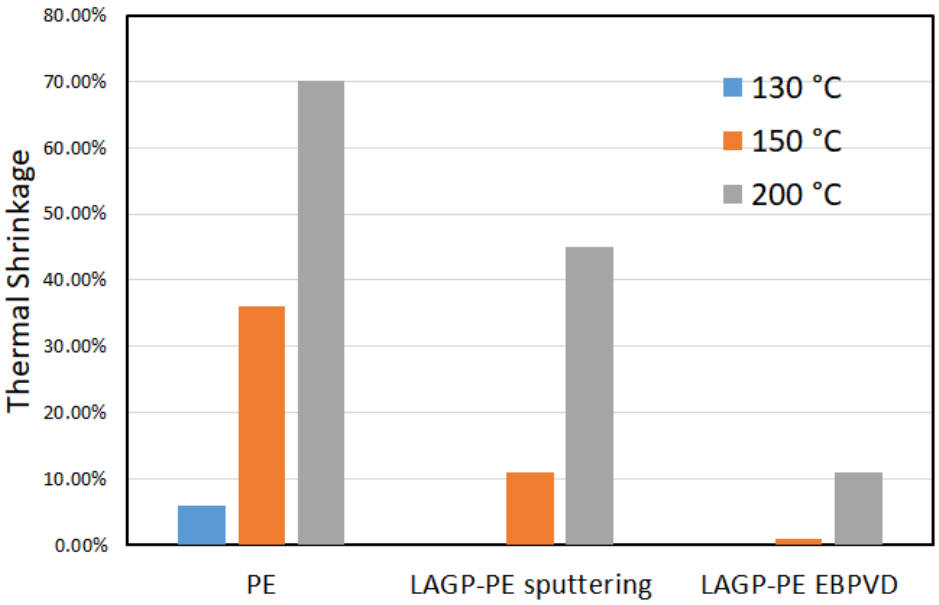

Figure 4. Thermal stability of separators up to 200°C in air

The thickness of LAGP layer on PE separator determines their thermal stability, as shown in Figure 5. A 500 nm LAGP-coated on PE even by using sputtering technique shows no thermal degradation (shrinkage) when kept at 200°C for 2 hours.

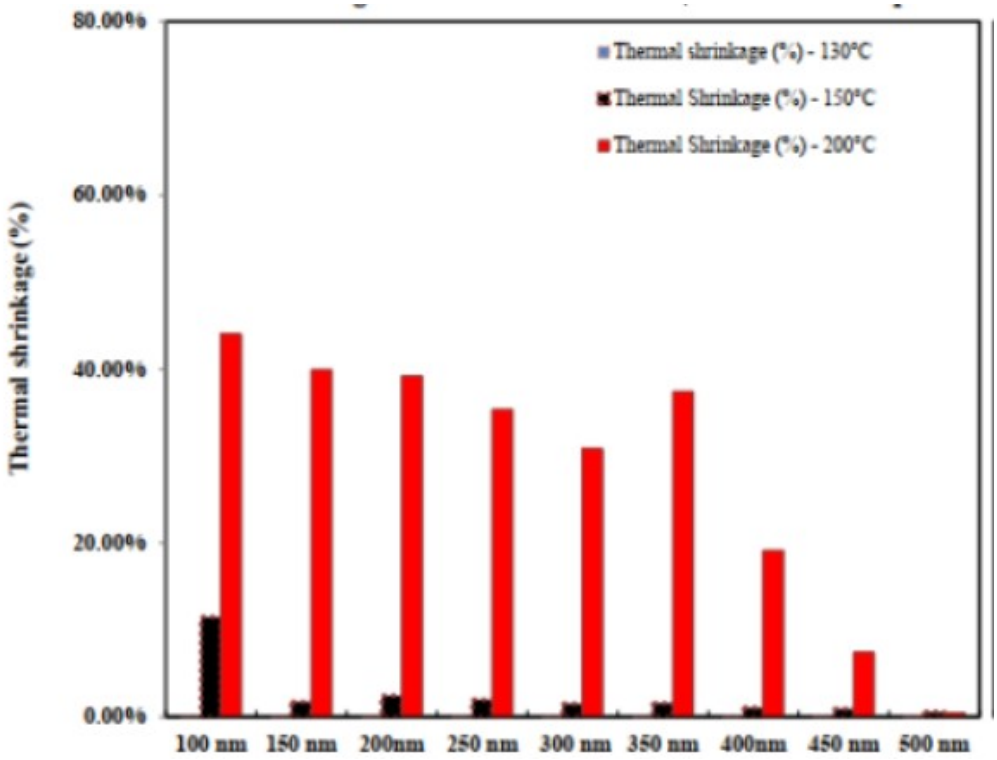

Figure 5. Dependence of Thermal stability on LAGP thickness

Figure 6 shows surface morphology of PE, 100 nm LAGP-coated PE by sputtering, and 100 nm LAGP-coated PE by EB-PVD before and after testing of their thermal stabilities at 150°C and 200°C for 2 hours in air. PE without ceramic coating melts completely around 150°C, LAGP-coated PE using sputtering starts shrinking at 150°C but melts completely at 200°C, and LAGP-coated PE using EB-PVD only starts shrinking at 200°C but does not melt at 200°C. This indicates that the ceramic coating has a strong positive effect on mitigating thermal shrinkage of the polymeric separators at temperatures above its melting point. This is probably due to two critical factors. Firstly, the ceramic layer contains no polymeric binder, so it is thermally stable at the annealing temperature of 200°C. Secondly, the deposited ceramic film binds strongly with the separator's fibers, and therefore provides mechanical supports to the structure of the polymer from collapsing during thermal exposure for an extended period of time (two hours). A two-hour delay in actual cell shorting can help evert thermal runaway events either by forced cooling, or by stopping battery operation using the BMS to program in specific cooling events as a function of time, or time-induced battery shutdown/cooling periods.

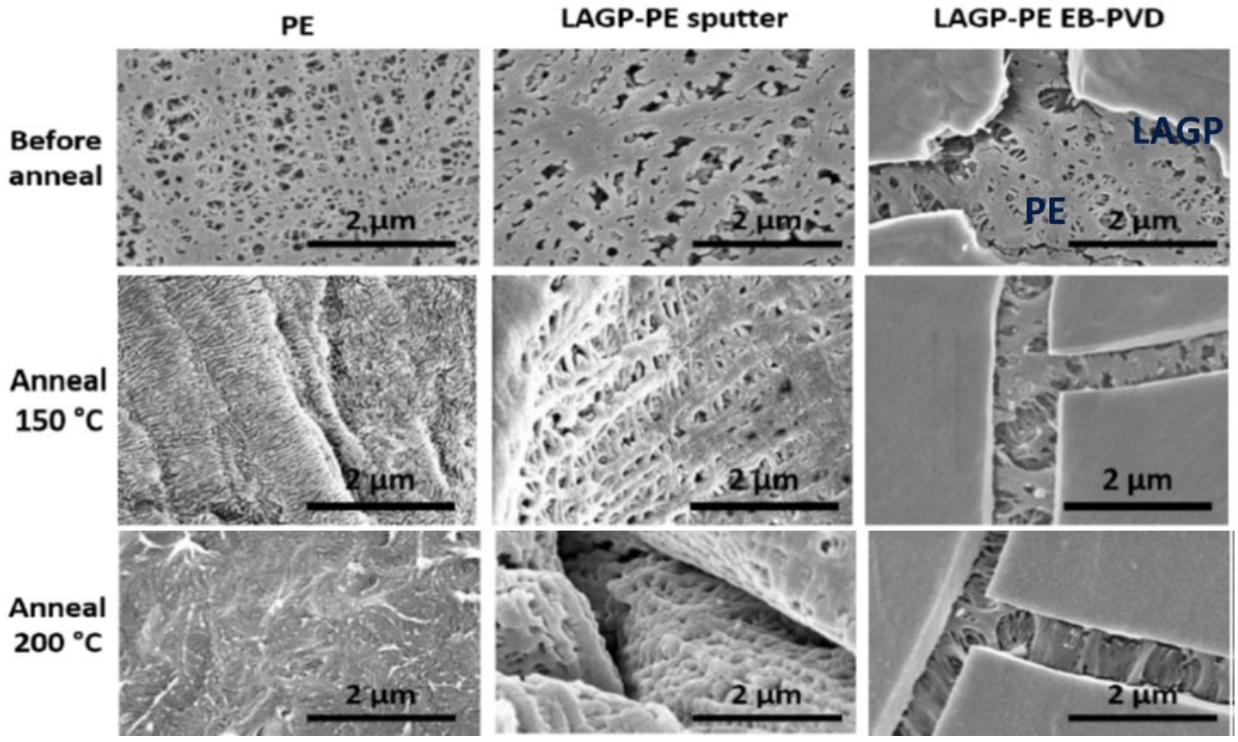

Figure 6. Stability of separator at 150°C and 200°C

Thermal stability of ceramic (LAGP) coated and pristine PE separators were also investigated in the presence of liquid electrolyte used in Li-ion batteries to understand the role of the separator in the thermal runaway process [10]. Figure 7 shows shutdown (separator pore closer) and breakdown (melting/fracture) behavior of separators up to a temperature close to 200 °C. During the shutdown temperature range, the pores of the separator close, which restrict flow of Li^+, and hence the resistance of the cell increases; at that time the BMS stops the functioning of the cell to avoid a battery thermal runaway process. However, sometimes the battery temperature can go past the separator breakdown point and melt the separator leading to the direct contact between electrodes, which leads to cell shorting. In this situation, Li^+ flows freely and provide low resistance path for high current flow that can internally heat-up the cell causing the thermal runaway process to begin. Therefore, it is generally agreed that a large difference between shutdown temperature and breakdown temperature improves battery safety. Clearly, all the commercial separators, including commercial ceramic-coated (2 µm Al_2O_3 coating using polymeric binder) PE, have a narrow temperature window between shutdown and breakdown, which is why the commercial separators are prone to not prevent the thermal runaway process. Though breakdown of commercial ceramic-coated (Al_2O_3 coating using polymeric binder) PE is slower than pristine PE. But, UDRI's LAGP coated separator developed during this project, even with 40 nm thick LAGP coated using EB-PVD, does not break down to a temperature >190°C. It

would be beneficial to test the thermal ability of LAGP-coated separators in contact with liquid electrolyte used in Li-ion cell beyond our present test capability of >200°C.

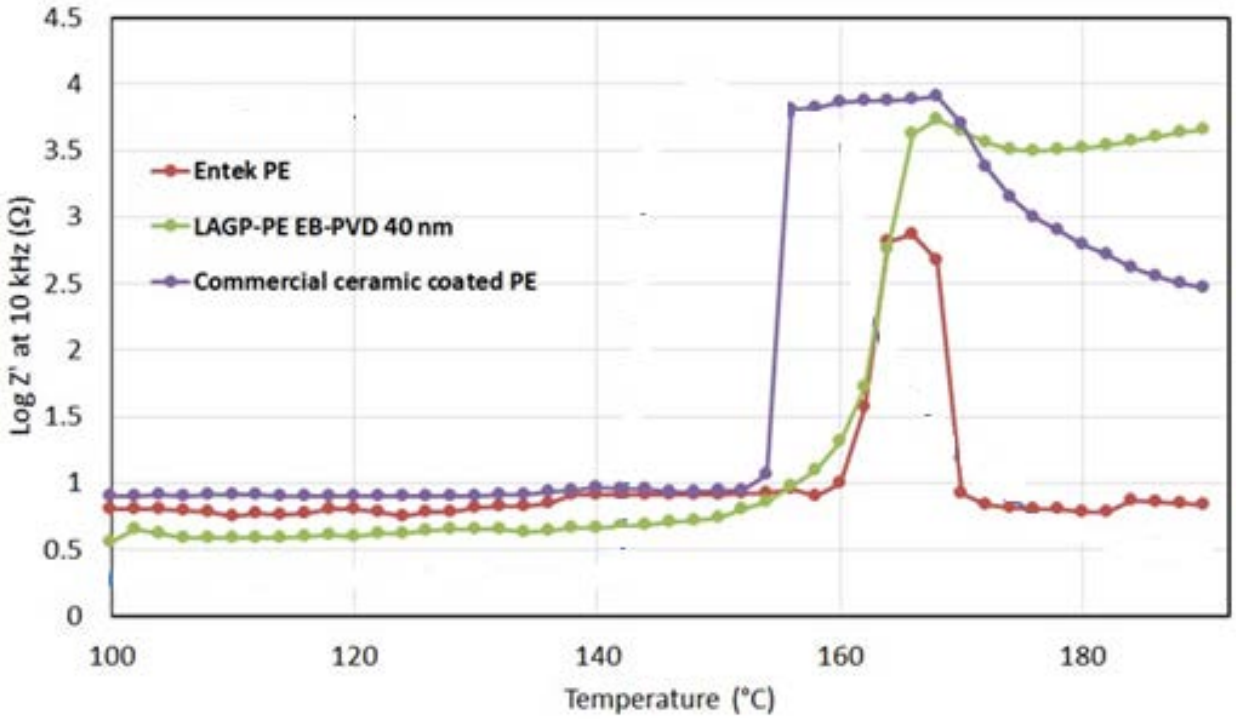

Figure 7. Separator shutdown and breakdown temperature

The post-test characterization of separator samples used in Figure 7 further confirms the superior thermal performance of UDRI's LAGP-coated PE separator (Figure 8). When tested till 190°C, PE separator fractures very badly, Al_2O_3-coated commercial PE starts fracturing at edge (red circle) and UDRI's LAGP (40 nm) coated PE does not fracture at all as also confirmed in Figure 8.

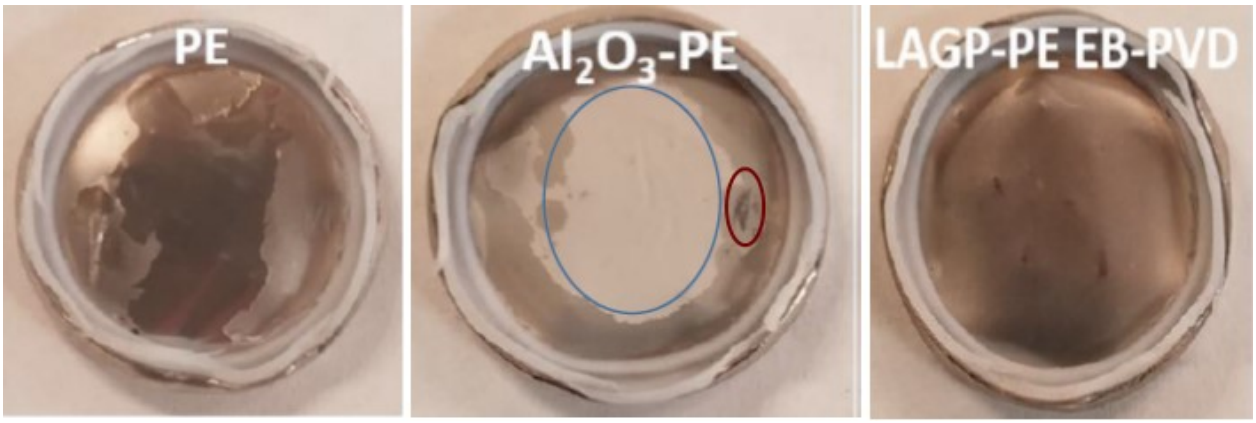

Figure 8. Pictures of separators after testing at 190°C in contact with liquid electrolyte

The fracturing of Al_2O_3 ceramic-coated commercial PE (Figure 8) starts with degradation of binder (usually polyvinylidene fluoride (PVDF) is used that starts dissolving in liquid electrolyte above 80°C) used to bind Al_2O_3 particles on commercial PE, followed by agglomeration of Al_2O_3 particles as seen in Figure 9, which then exposes a bare PE surface to high temperature. Figure 9 also shows that the structure of PE melted, whereas LAGP-coated PE is still intact confirming the superior thermal stability. No degradation of the LAGP layer on PE beyond 190°C highlights the importance of binder-less ceramic coating developed during this project using EB-PVD and sputtering techniques.

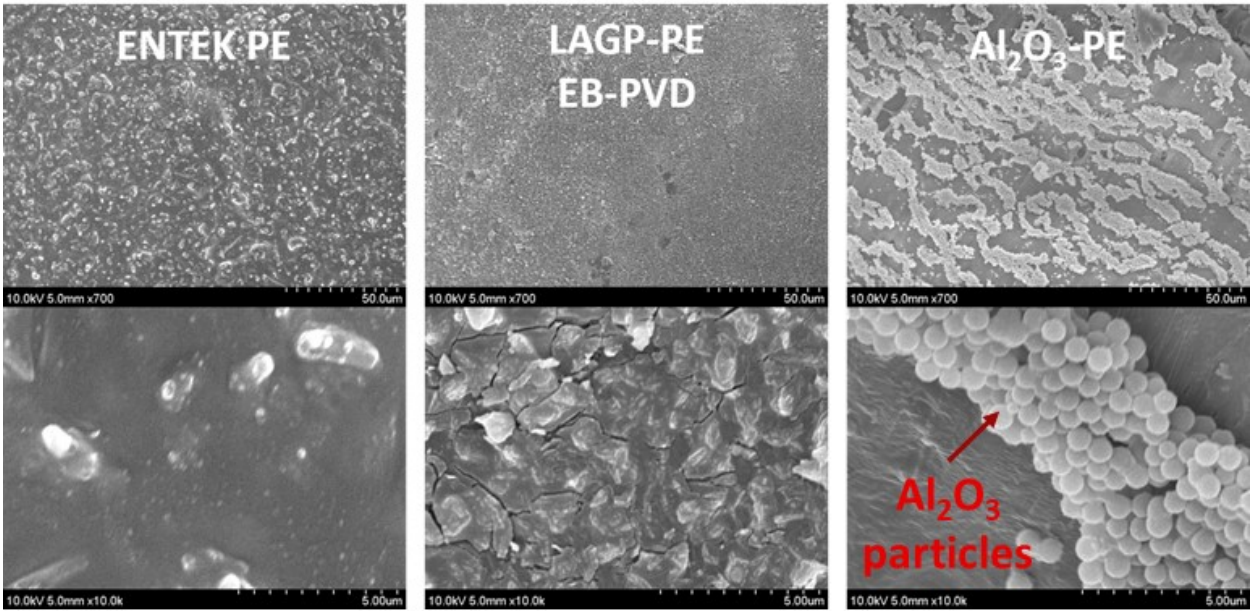

Figure 9. Surface morphology of separators after testing until 190°C

Figure 10 shows the effect of ceramic coating (LAGP) on the electrical performances of LAGP-coated separator versus pristine PE separator soaked in common liquid electrolyte (1M $LiPF_6$ in ethylene carbonate (EC):ethyl methyl carbonate (EMC): dimethyl carbonate (DMC)) in a temperature range of 0°C to 100°C. It can be clearly seen from Figure 10 that the conductivity of the LAGP-coated separator using EB-PVD is an order of magnitude higher suggesting that the LAGP layer assist in faster Li^+ conduction. It is known that the commonly used liquid electrolyte in Li-ion such as 1M $LiPF_6$ in EC:EMC:DMC is not stable beyond 80°C, which can be seen in a conductivity drop at 100°C. This implies that to achieve better electrical performances of separator and liquid electrolyte system together, the thermal stability of both the constituents matter.

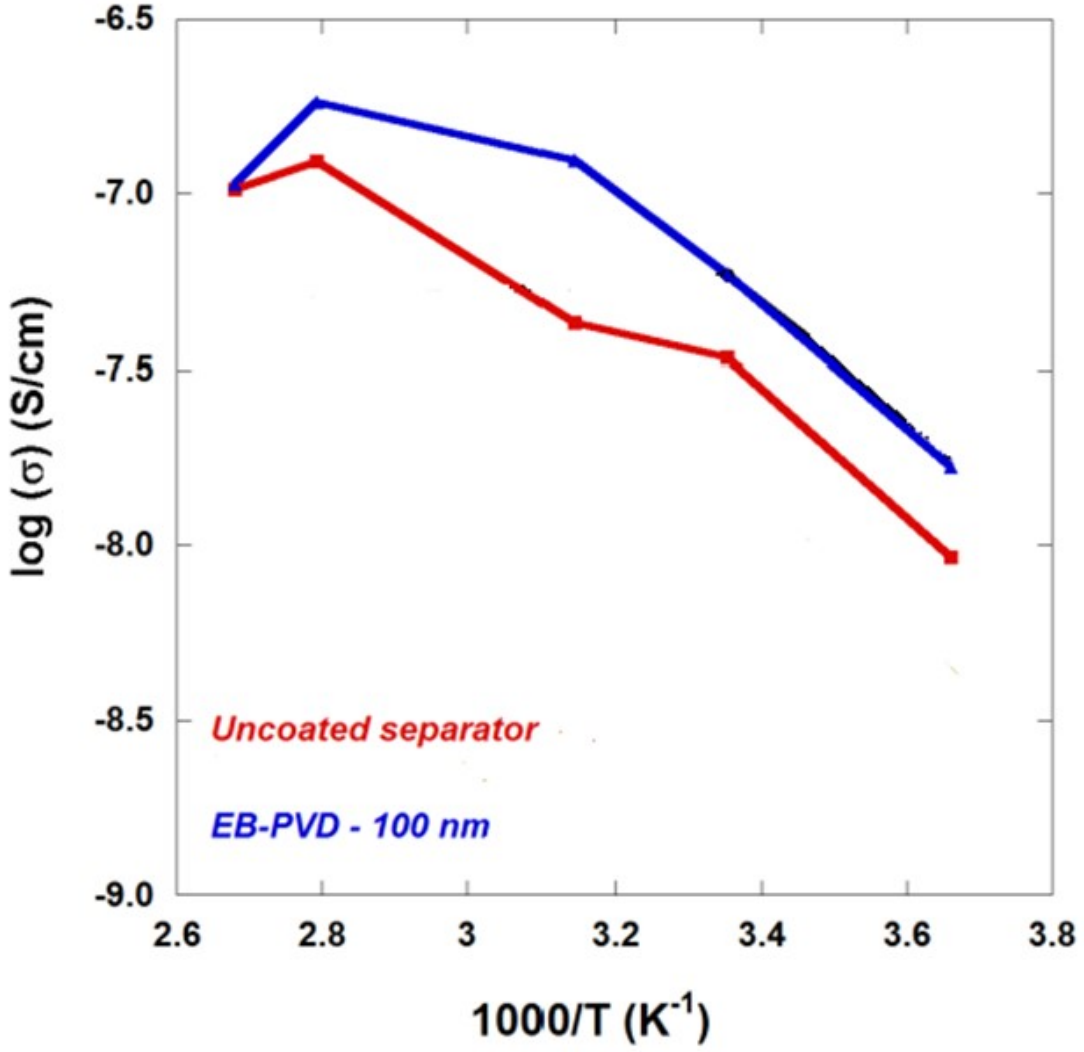

Figure 10. Temperature dependent conductivity of the uncoated and LAGP-coated (EB-PVD; 100 nm) PE separators soaked in liquid electrolyte

The cycling performance of UDRI's LAGP-coated separator versus bare PE separator in a full Li-ion cell (anode – graphite, cathode - $LiNiMnCoO_2$ (NMC), and electrolyte - 1M $LiPF_6$ in EC:EMC is shown in Figure 11. For this experiment, a LAGP with 200 nm thickness was coated on both sides of PE separators. Reproducible data showing a noticeable improvement in cycling performance was observed (see Figure 11).

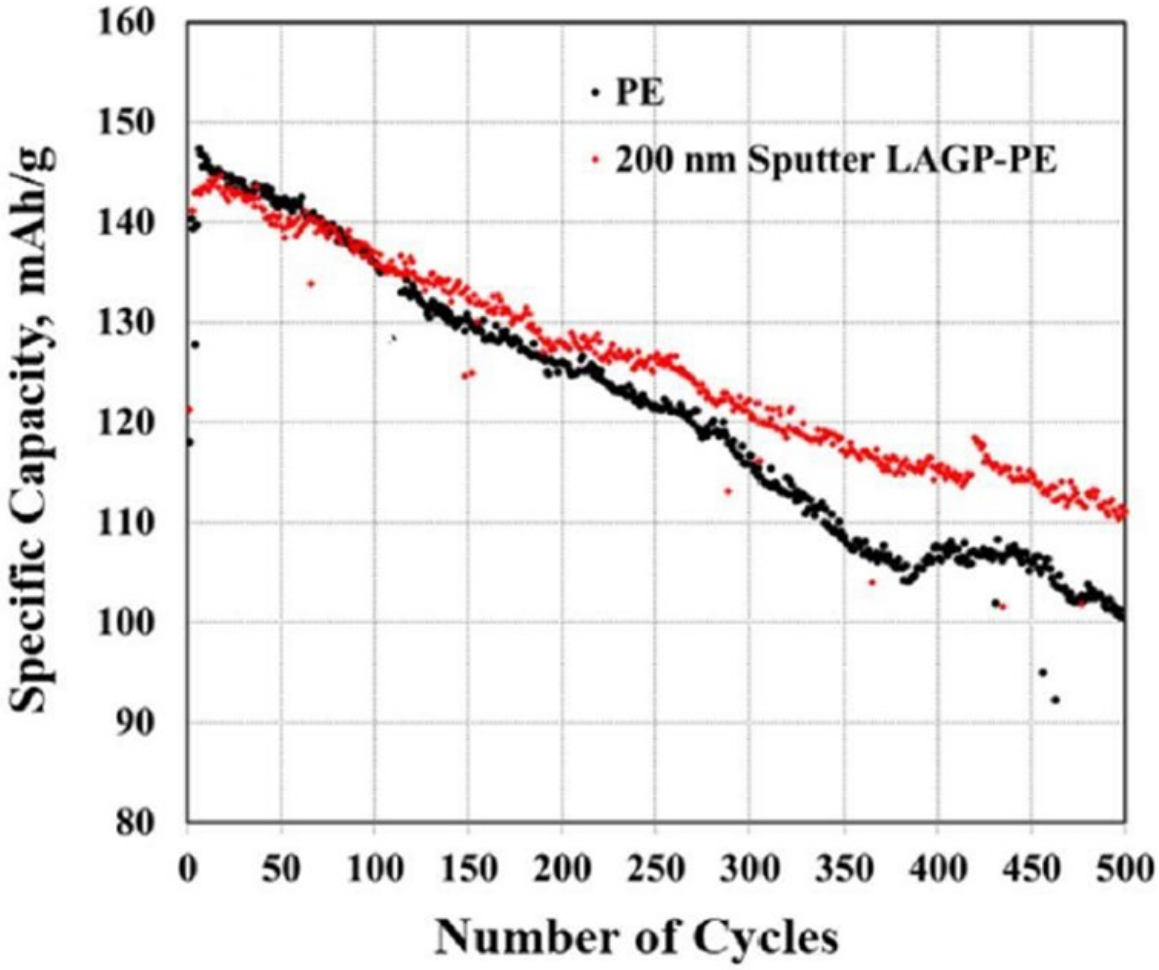

Figure 11. Cycling performance of UDRI's LAGP-coated PE versus bare PE separator in a standard Li-ion cell configuration

Dependency of Li-ion cell cycling performance depends on LAGP thickness (Figure 12). The LAGP layer modifies the pore structure of PE separator. A thicker coating may block some of the pores of separator and impede Li^+ transport and hence reduce cell performance. It's worth noting here that the thermal stability increases with LAGP thickness (Figure 5), whereas cycling performance initially increases with LAGP layer thickness to attend a maximum around 200 nm

when sputtering techniques is used, (100 nm LAGP was maximum when EB-PVD technique was used) and starts decreasing as thickness of LAGP increases as shown in Figure 12.

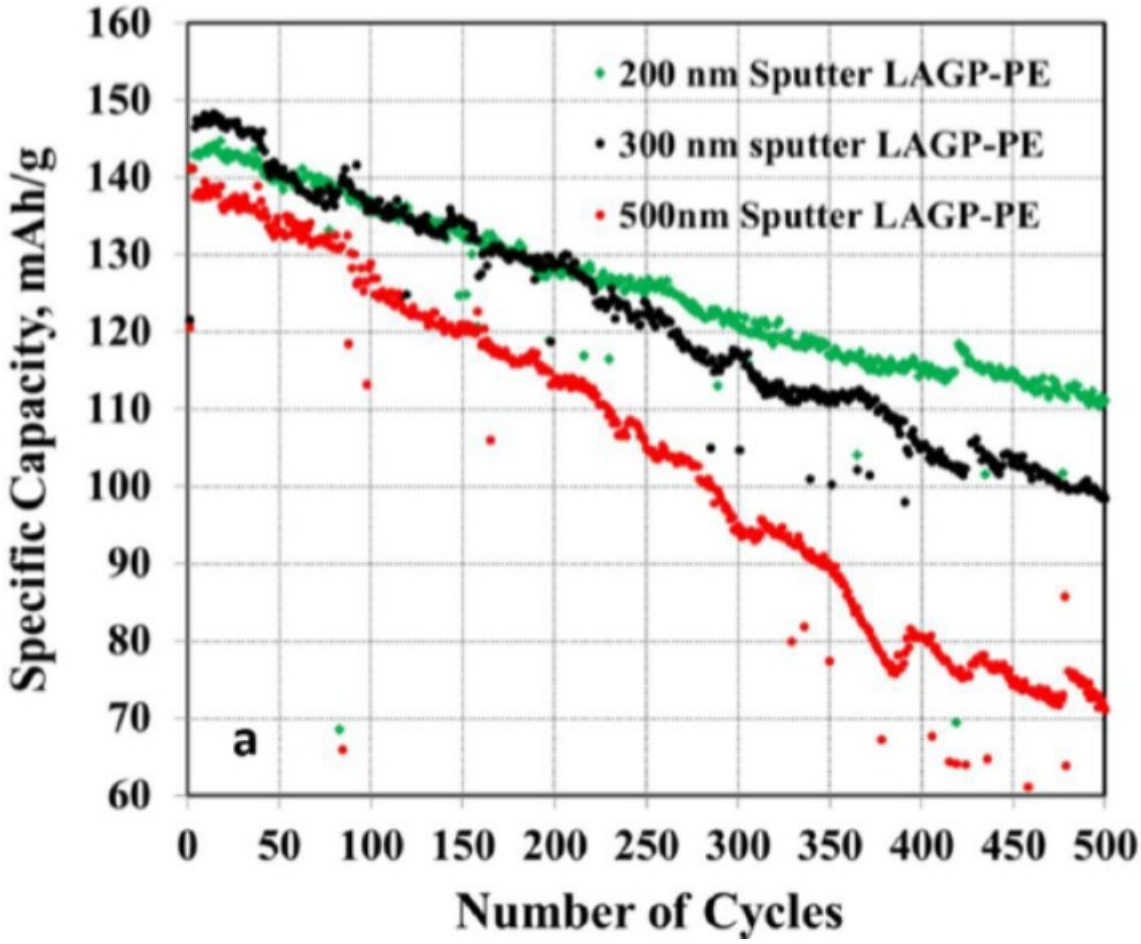

Figure 12. Cycling performance of Li-ion cells with different thickness of LAGP layer on PE separator

Cycling performance of LAGP-coated PE also depends on techniques used to fabricate LAGP layer on PE separator. Figure 13 shows the cycling performance difference of a 40 nm LAGP coated on PE using EB-PVD and Sputtering. This difference is mainly due to the fact that EB-PVD provides more surface coverage compared to sputtering for a given LAGP thickness (Figure 3). Better surface coverage is good for thermal performance but compromises with electrochemical performance unless LAGP is crystallized. Thus, an optimum LAGP layer is good for both thermal and electrochemical performances compared to bare PE separator.

Commercial Li-ion cells are designed to work best around room temperature; below 0°C and above 60°C Li-ion loses cell performance rapidly [11]. We selected a temperature that is much

higher (85°C) to determine if LAGP coating plays any positive role when cells are cycled at elevated temperature, where fast cell degradation is expected. Figure 14 shows a better cycling performance of Li-ion cell using LAGP-coated PE compared to Li-ion cell using bare PE separator. This shows the LAGP not only makes the PE separator thermally stable, but also improves cell performance at higher temperature. A much better cell cycling performance is expected if LAGP-coated PE is used with electrolyte that has higher thermal stability compared to normally used electrolyte (1M $LiPF_6$ in EE/EMC/DMC).

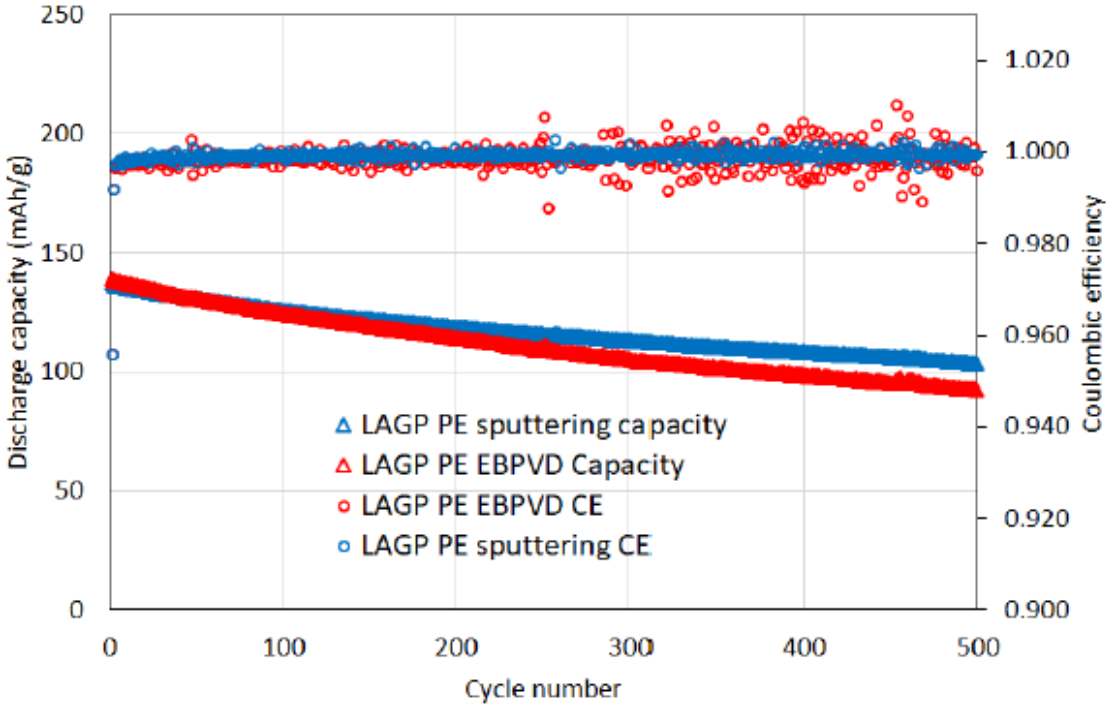

Figure 13. Cycling performance of Li-ion cells using LAGP-coated PE separators prepared using sputtering and EB-PVD process

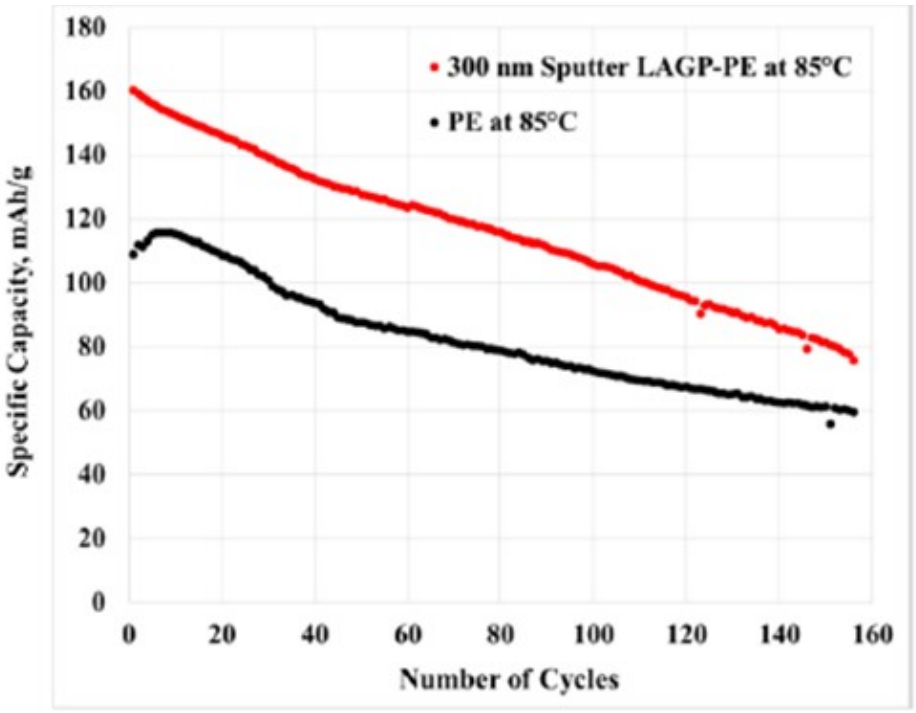

Figure 14. Cycling performance of 300 nm Sputter-coated LAGP-PE separator compared to plain PE separator at 85°C

2.1.2 Commercial ceramic electrolytes on Entek separator

Apart from LAGP, we also investigated a few other ceramic solid electrolyte, such as lithium lanthanum zirconium oxide (LLZO) and lithium tin phosphorus sulfide (LSPS). LLZO has shown better stability with Li compared to LAGP and LSPS, but LLZO [7] needs very high temperature of sintering (>1000°C) compared to >600°C for LAGP and >350°C for LSPS [8]. Also, Li^+ conductivity of LLZO is slightly inferior compared to LAGP (see Figure 15) and LSPS. On the other hand, LSPS is not very stable in normal atmospheric conditions and always requires handling inside an inert gas filled glove box [7, 8]. Given the property variations among these materials, we decided to test both LLZO and LSPS to compare performance with LAGP coating.

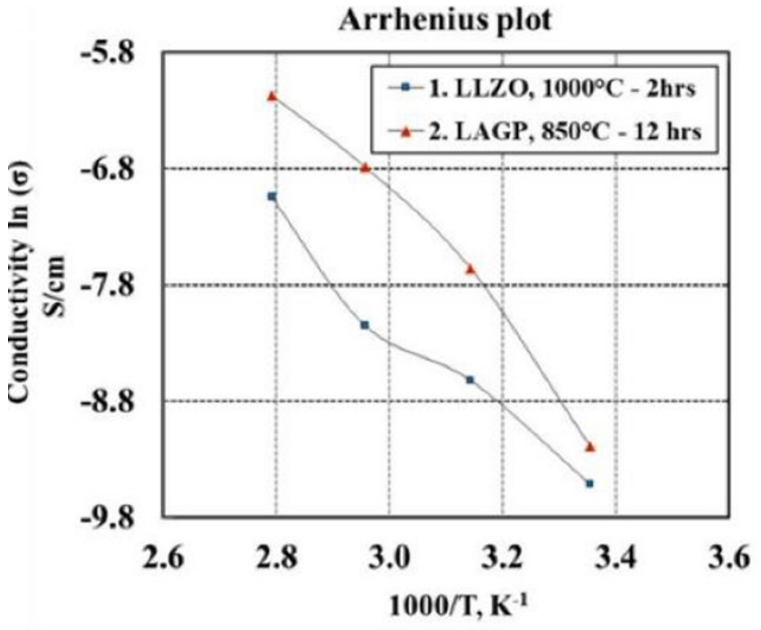

Figure 15. Comparative conductivity of LAGP and LLZO

As with LAGP, we coated LLZO (20 nm – 500 nm) using EB-PVD. Figure 16 shows morphology of a) 20 nm, b) 100 nm and c) 200 nm LLZO at PE separator. Unlike LAGP (Figure 3), a 20 nm LLZO coating does not change the separator morphology much. However, as the thickness of LLZO increased to 100 nm and 200 nm and beyond, the LLZO starts to cover more and more separator surface. The surface morphology difference between LAGP and LLZO may be due to their different melting temperatures that affects rate of depositions, and also due to different growth mechanisms.

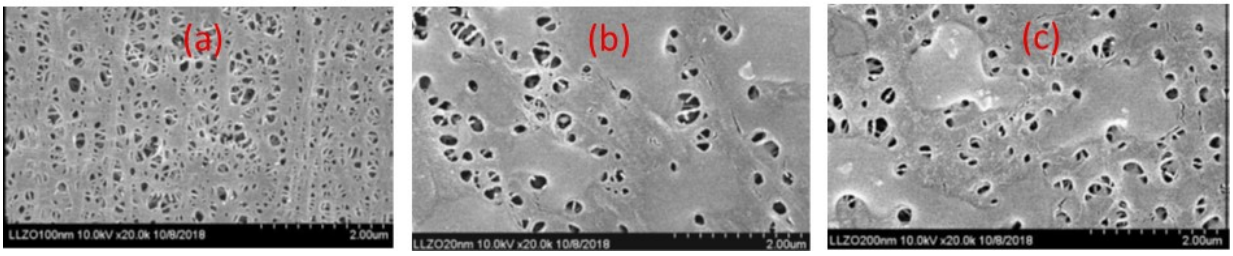

Figure 16. Morphology of LLZO-coated on PE separator with different thickness

Figure 17 shows the thermal stability of 200 nm and 400 nm LLZO on PE compared to LAGP on PE. It can be seen that 200 nm LLZO/PE shrinks to around 45% whereas 200 nm LAGP shrinks to below 40% when both samples were kept at 200°C for 2 hours. However, at 400 nm both LAGP and LLZO show very similar thermal stability. A slight inferior thermal stability with 200

nm LLZO can be correlated to lower PE surface coverage by LLZO and LAGP (Figure 3 and Figure 16).

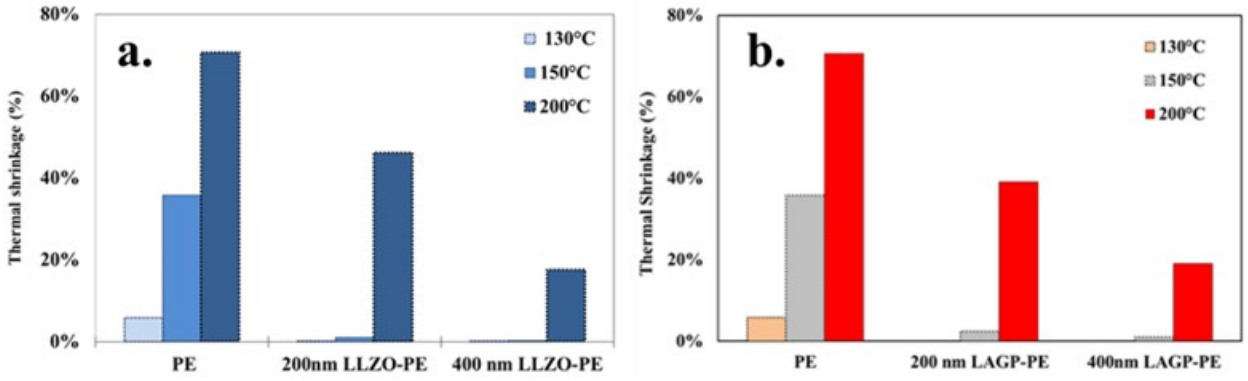

Figure 17. Thermal stability of LLZO and LAGP-coated separators

Figure 18 shows Li-ion cell cycling using LLZO-coated PE separators. All the other cell components remain the same, as in the study of LAGP-coated PE separator. It can be seen that cell performance increase as LLZO coating increases from 20 nm to 200 nm (EB-PVD), and a similar trend was observed with LAGP. Again thicker coating (for example 200 nm vs 400 nm) is good for thermal stability (Figure 17) but compromises the electrochemical performance (Figure 18 – 200 nm vs 400 nm, sputter-coated samples). A 200 nm LLZO is a good compromised version for both decent thermal stability and optimal cell cycling performance.

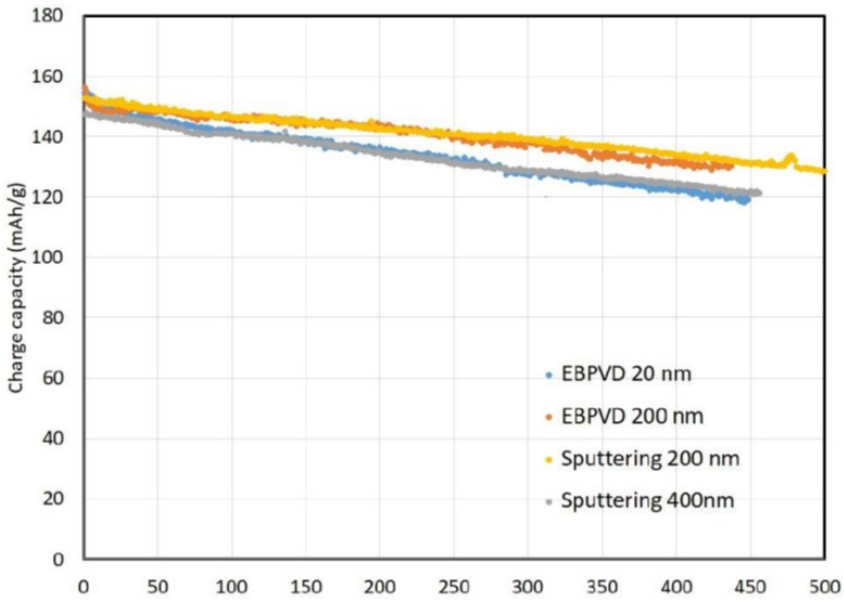

Figure 18. Long-term cycling of LLZO-coated PE in Li-ion cell

As aforementioned, we also conducted similar tests on sulfide solid electrolyte (LSPS), which has better conductivity compared to both LAGP and LLZO but inferior environmental stability. Since the EB-PVD and sputtering requires exposure of sample in normal conditions at least for a short period of time (few minutes) during sample loading in the machine and taking sample out of the machine, we took the utmost care to minimize atmospheric exposure of sulfide material during the coating process. Figure 19 shows samples from thermal stability tests. Rows 1 through 3 (Figure 19) are LSPS-coated samples (20 nm, 40 nm, and 80 nm) exposed to temperature up to 200°C for 2 hours. Unlike LAGP and LLZO, all the LSPS-coated samples shrank up to 60%, only slightly better than bare PE (70% shrinkage). The superior thermal stability with LAGP over LSPS can be seen in row 4 of Figure 19, where a combination of 20 nm LAGP and 20 nm LSPS was fabricated on PE separator and thermal stability improved drastically.

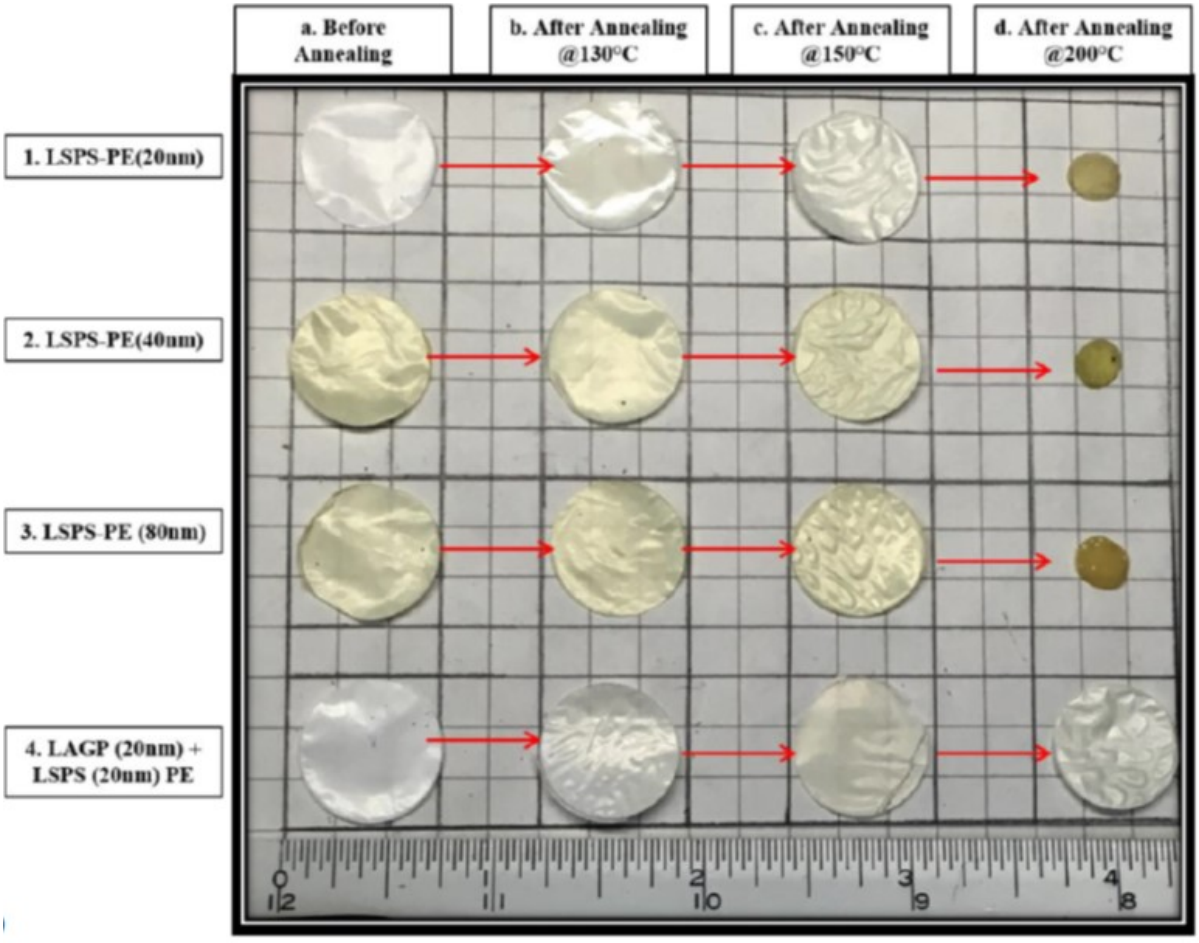

Figure 19. Thermal stability of LSPS and LAGP/LSPS-coated PE up to 200°C

Figure 20 shows the cycling performance of Li-ion cells using LSPS and LAGP/LSPS-coated PE separators. All cells degrade at similar rates, indicating that the coating has little influence on the degradation mechanism of the cells. The performance is poorer than without coating or with LAGP and LLZO coating, suggesting that the coating layer has an adverse effect on the electrochemical performance of lithium ion batteries (LIBs).

We have also tested the separator coated by 20 nm of LAGP and then 20 nm of LSPS, both with EB-PVD. It was clear that cell performance with the hybrid coating was substantially better than LSPS coating alone. Therefore, it appears that the improvement in cycling performance was mainly due to the LAGP coating and protection of LSPS, as otherwise LSPS may have suffered from environmental degradation.

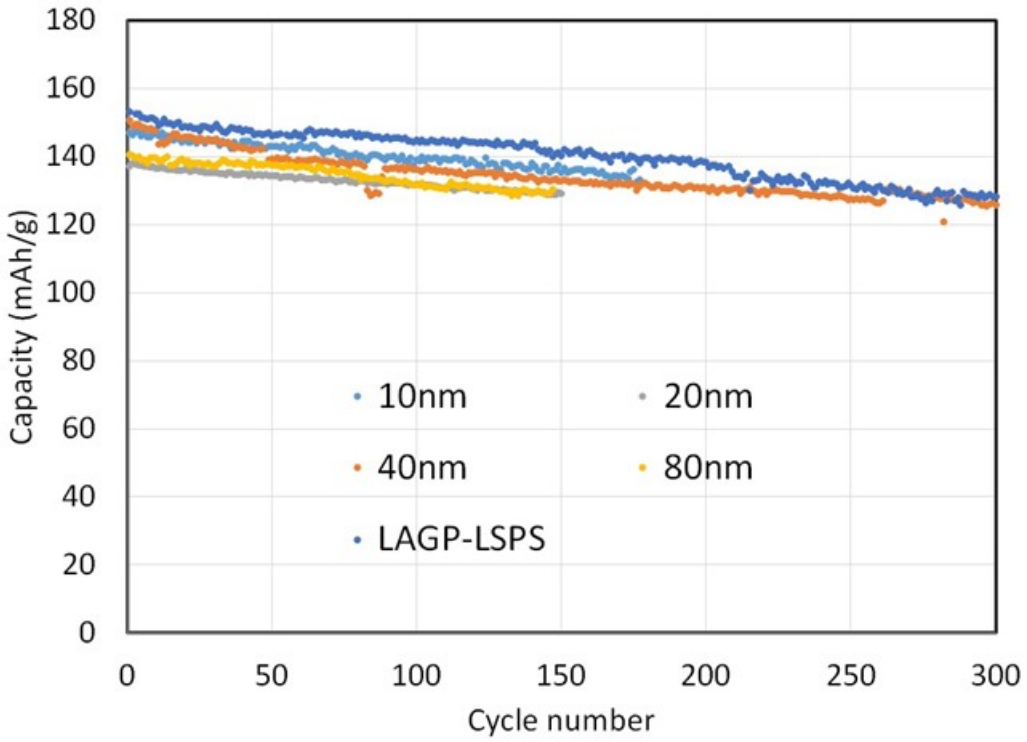

Figure 20. Li-ion cell cycling using LSPS and LAGP/LSPS-coated PE separators

2.1.3 Insulating ceramic electrolyte on Entek separator

So far only insulating ceramics like Al_2O_3 have been used to make commercial separators with better thermal stability compared to bare PE separators [9]. Unlike the process developed for thin-film ceramic deposition without use of any binder in this project, commercial ceramic coating is done using slurry casting method, where slurry of ceramics are mixed with polymeric

binder and casted on PE or any other Li-ion separators. Slurry coating allows fabrication of only thick ceramic layers, usually 1-2 µm. As thicker ceramic layers negate energy density and at same time the coating layer survives only to a limited temperature (<80°C), due to binder dissolving into the battery liquid electrolyte, we investigated a *binder-free, thin-film (20-500 nm)* Al_2O_3 coating using EB-PVD technique. EB-PVD fabrication of Al_2O_3 was similar to thin-film deposition of LAGP. Moreover, slurry-coated ceramic layers are still porous unlike even 100 nm Al_2O_3-coated using EB-PVD (Figure 21), and in the event of dendrite growth, slurry-coated Al_2O_3 separator may not be very effective.

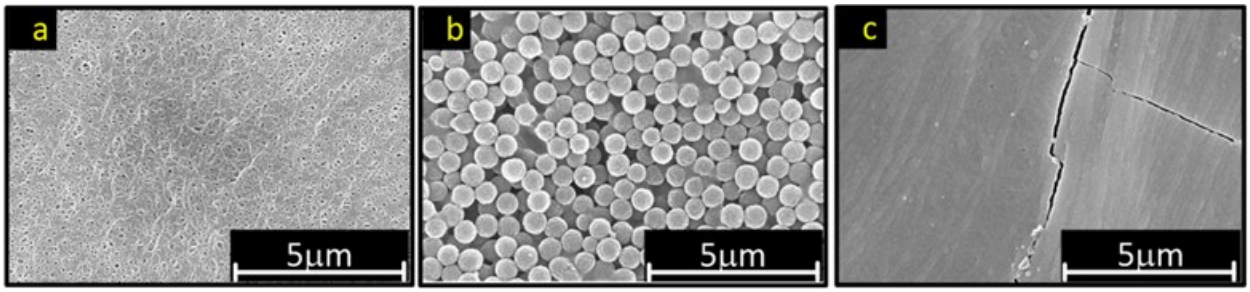

Figure 21. SEM surface morphology for a) Pristine PE separator, (b) commercial Alumina PE separator (Al_2O_3 layer thickness 1-2 µm), (c) EB-PVD coated Al_2O_3-PE (Al_2O_3 layer thickness 100 nm)

Figure 22 shows thermal stability of PE, commercial Al_2O_3-coated PE, and EB-PVD coated Al_2O_3-PE (100 nm), after being annealed at 130°C, 150°C, and 200°C temperature. Clearly, a 100 nm Al_2O_3-coated PE using EB-PVD technique, and developed during this project, is far more thermally stable as compared to commercially available separators including thick (2 µm) Al_2O_3-coated PE.

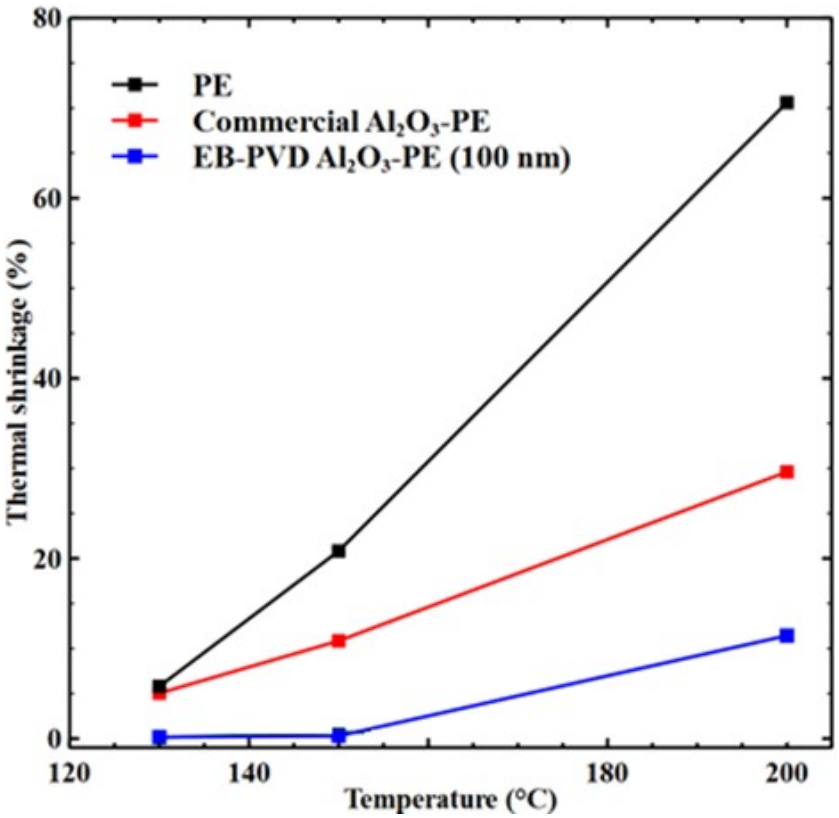

Figure 22. Thermal stability of commercial versus EB-PVD coated Al_2O_3-PE (100nm)

The thermal stability advantage of thin-film Al_2O_3 coating on PE developed during this project is further evident in Figure 23, which shows separator shutdown and breakdown behavior when used in liquid electrolyte. Breakdown behavior of commercial Al2O3-coated PE is better than bare PE, but quite inferior to UDRI's 100 nm Al2O3-coated (binder-free) PE using EB-PVD.

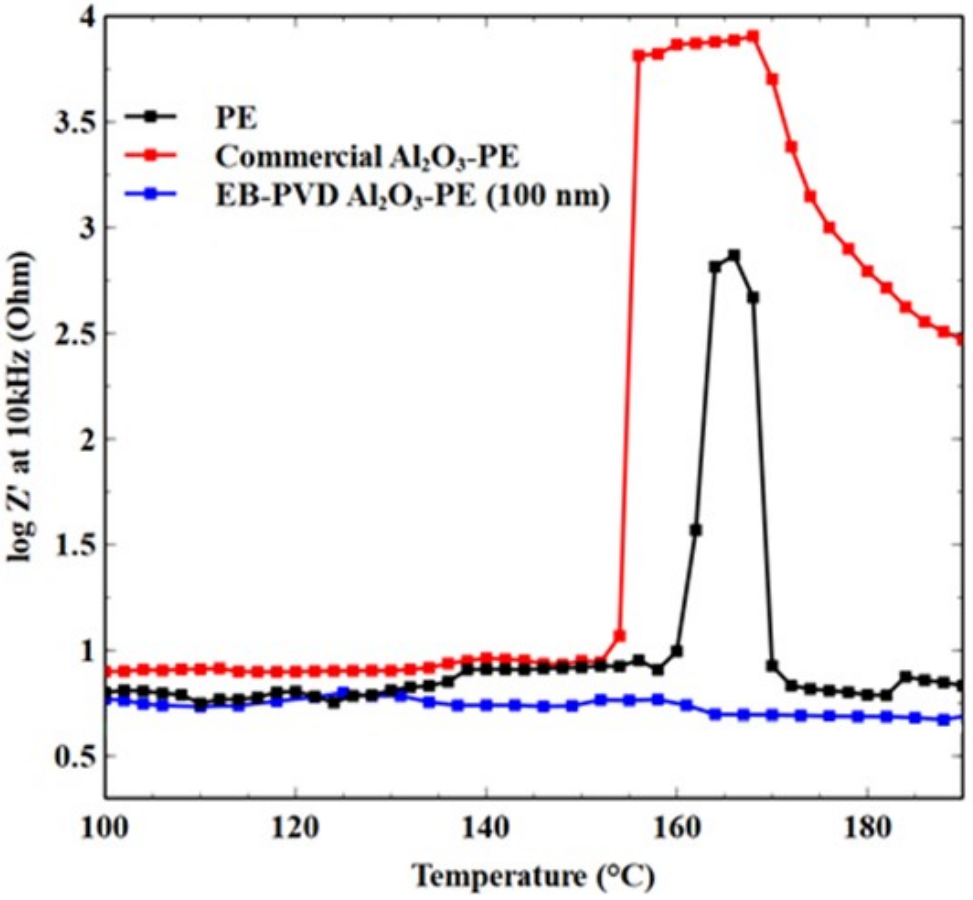

Figure 23. Separator breakdown temperature

UDRI's **100 nm** Al_2O_3 coating remains intact beyond 190°C, whereas commercial **2 µm** Al_2O_3 coating dissolves out when tested with Li-ion liquid electrolyte up to 190°C (Figure 24). The reason for improvement in UDRI's Al_2O_3 coating on PE (binder-free, better adhesion, etc.) is its similarity to LAGP-PE separators.

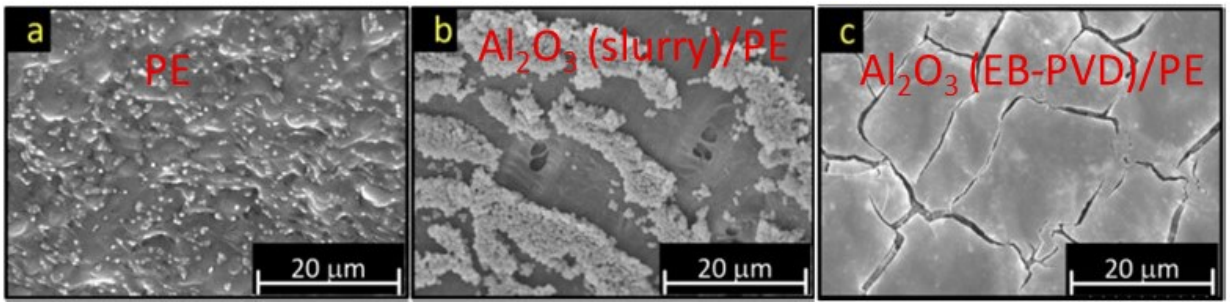

Figure 24. Post thermal test characterization of separators

The easy dissolution of the Al_2O_3 layer in commercial separator is further verified by a peel test. To compare the adhesion strength between the ceramic coatings with the polymer membranes, a simple tape peeling test was performed on the separators. Briefly, a piece of scotch tape was pressed on the separator with the same force and then peeled off. Figure 25a & 25c show scanning electron microscopy (SEM) images of the border regions of the commercial 2 μm Al_2O_3-PE and UDRI's EB-PVD coated 100 nm Al_2O_3-PE. Figure 25b & 25d show the tape side after the peel test. For the commercial Al_2O_3-PE separator, due to the low adhesion strength of the Al_2O_3 particles with the PE, all of the particles came off the polymer layer and were stuck to the tape surface. This detachment of the ceramic layer suggests a weak bonding and low interfacial integrity between the ceramic layer and polymer. For the EB-PVD coated Al_2O_3-PE, there was no change in the morphology before and after conducting the peel test. This suggests that the Al_2O_3 particles are strongly bonded to the polymer membrane when deposited using EB-PVD.

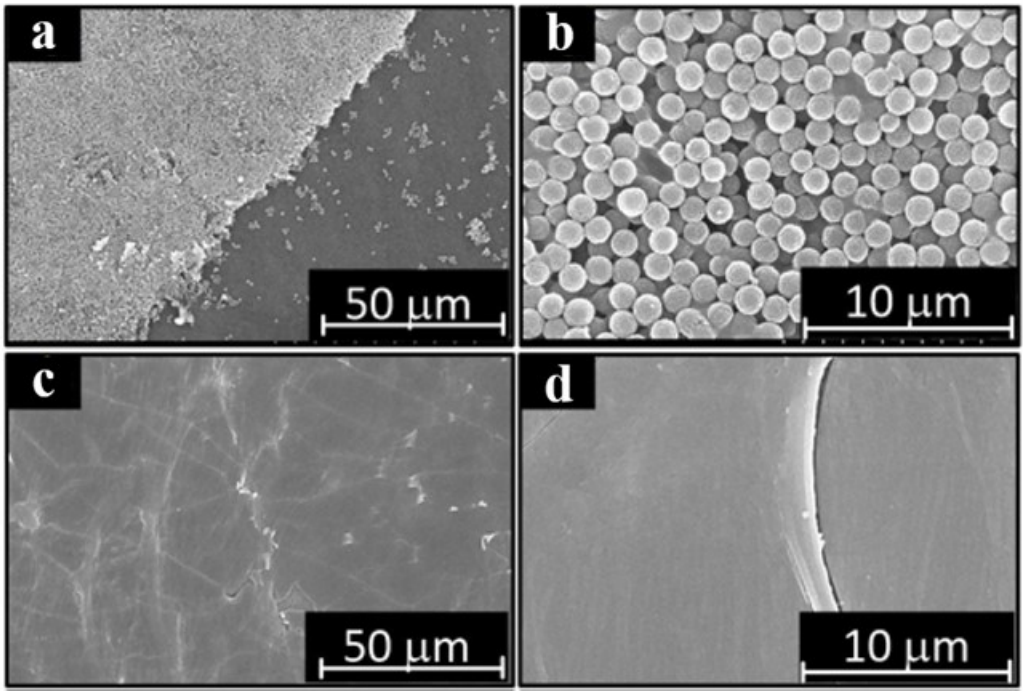

Figure 25. Al_2O_3 layer adhesion test

Furthermore, UDRI's 100 nm Al_2O_3 on PE (EB-PVD) shows competitive cell cycling performance (see Figure 26). In summary, Al_2O_3 coating by EB-PVD has many beneficial effects on the properties of PE separators, similar to LAGP and LLZO coating. It is significantly more effective at improving the thermal stability of PE separators than commercial Al_2O_3-coated

separators. The adhesion of Al_2O_3 layer to the PE separators is much superior to that on commercial Al_2O_3-coated separators. Thin Al_2O_3 coating impedes cell impedance only slightly, but has a beneficial effect on LIB cycling stability.

It is important to note that Al_2O_3 is cheaper than LAGP and LLZO, but insulating in nature. Thus, the thickness of Al_2O_3 always needs to be less. If high thickness of ceramic is required, especially to improve dendrite prevention, LAGP and LLZO should be preferred. LAGP and LLZO being Li^+ conductors, after annealing (as discussed in next section) can provide further advantage in yielding better cell cycle-life performance in addition to dendrite prevention, as LAGP and LLZO are single Li^+ conductors (discouraging transport of any species other than Li^+). Thus, the selection of LAGP and LLZO versus Al_2O_3 will depend on end use and cost.

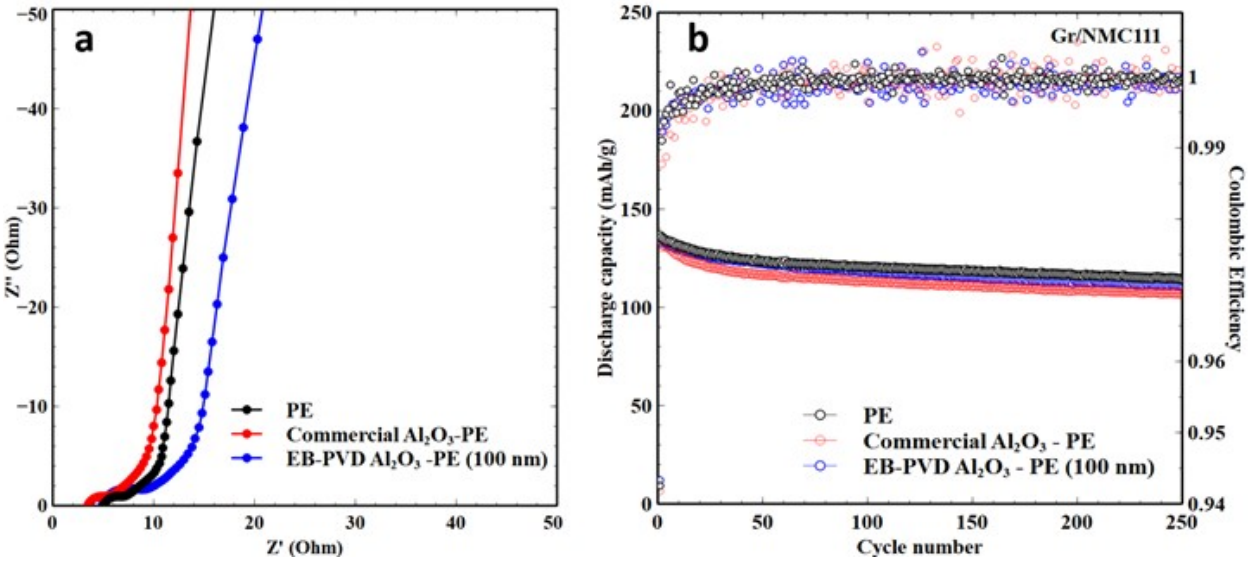

Figure 26. Electrical and Li-ion cell cycling performance comparison

2.1.4 UDRI's ceramic electrolyte on polyimide separator

The results presented in sections 2.1.1 to 2.1.3 suggest that the thermal and electrochemical performances of UDRI's thin-film ceramics-coated PE, either using EB-PVD or Sputtering, are comparable regardless of using LAGP (Li^+ conducting ceramic), LLZO (Li^+ conducting ceramic) or Al_2O_3 (insulating ceramic). The exception is LSPS (Li^+ conducting ceramic), which significantly degrades when exposed to normal atmosphere. With use of active ceramic (LAGP and LLZO), even better electrochemical performance was expected compared to commercial PE or Al_2O_3 (insulating ceramic) coated PE. One reason for this may be the fact that deposited ceramics using EB-PVD and sputtering are amorphous in nature [4]. In an amorphous state, even

LAGP and LLZO are Li^+ insulating. To make LAGP and LLZO layer Li^+ conducting, the ceramic-coated separator must be annealed at elevated temperature. In bulk form, LAGP and LLZO crystallize well at around 850°C and 1100°C, respectively. In thin-film form, LAGP and LLZO may crystallize 200-300°C below their bulk crystallization temperatures. Regardless, PE used as LAGP and LLZO support cannot survive even a temperature above 200°C, therefore there is no possibility of crystallizing LAGP and LLZO deposited on PE if one wishes to make LAGP and LLZO Li^+ conducting and further improve the electrochemical performance of the coated separators. In order to crystallize LAGP and LLZO, PE must be replaced with a thermally stable polymeric separator. Polyimide (PI) [12] is the only commercially available separator [Jiangxi Advanced Nanofiber S&T Co.] that can survive a temperature above 400°C, but it degrades very fast when the temperature is raised toward 500°C (see Figure 27). The thermal stability of PI separator can be further improved by UDRI's thin-film LAGP or LLZO coating depending on the LAGP or LLZO thickness (see Figure 28), but can still fall short in improving thermal stability to a desired temperature that can allow complete crystallization of LAGP layer. However, a partial crystallization of UDRI's thin-film LAGP on PI is possible at 400°C.

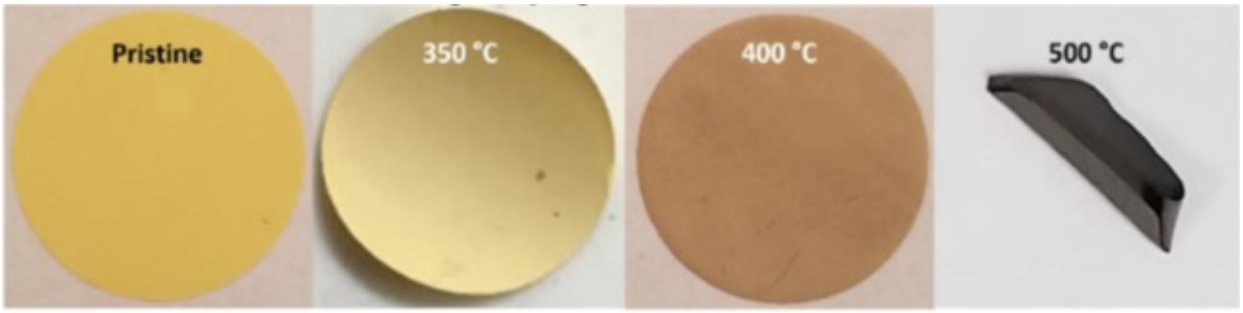

Figure 27 One hour thermal stability of PI in Argon atmosphere

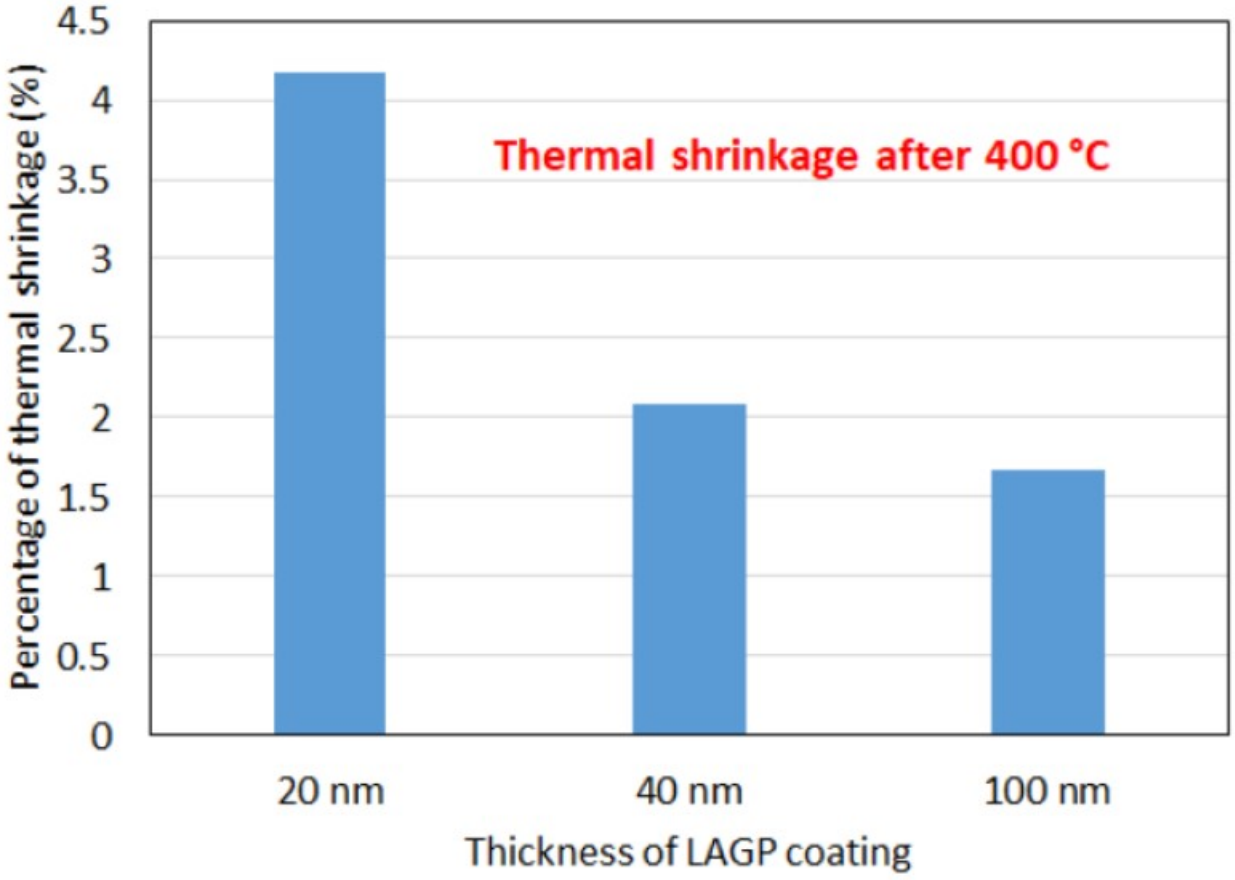

Figure 28. Thermal stability of LAGP-coated (EB-PVD) PI separators at 400°C

Figure 29 shows partial crystallization, in X-ray diffraction (XRD) plots, of a 500 nm LAGP-coated PI separator at 400°C (1 h); however, there is no crystallization of the LAGP layer at 350°C. The partial crystallization of LAGP at 400°C is further confirmed by SEM study (as seen in Figure 30), where LAGP layer at 350°C looks flat but bubble-like features (partially crystalline material) start appearing at 400°C. Complete crystallization of LAGP layer could not be achieved as PI degrades beyond 400°C.

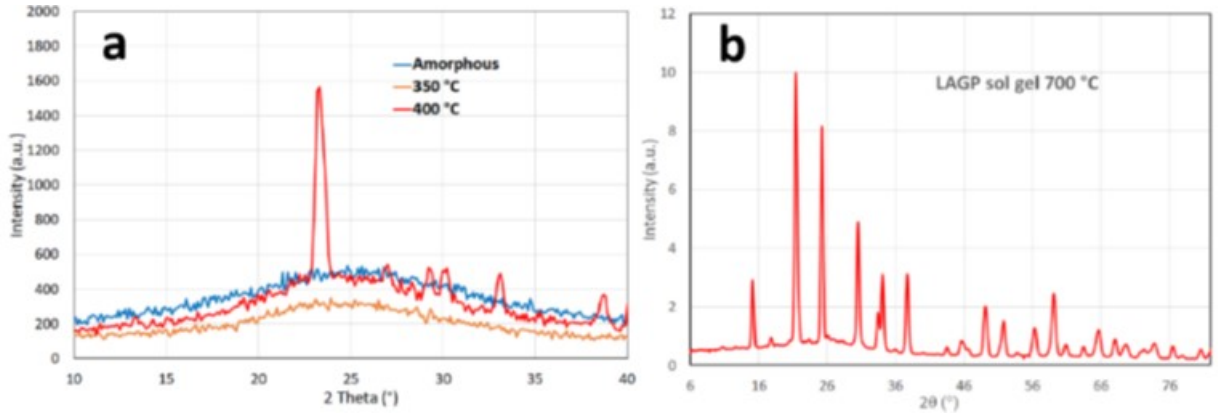

Figure 29. XRD pattern of LAGP-coated PI crystallized up to 400°C and bulk LAGP material crystallized at 700°C

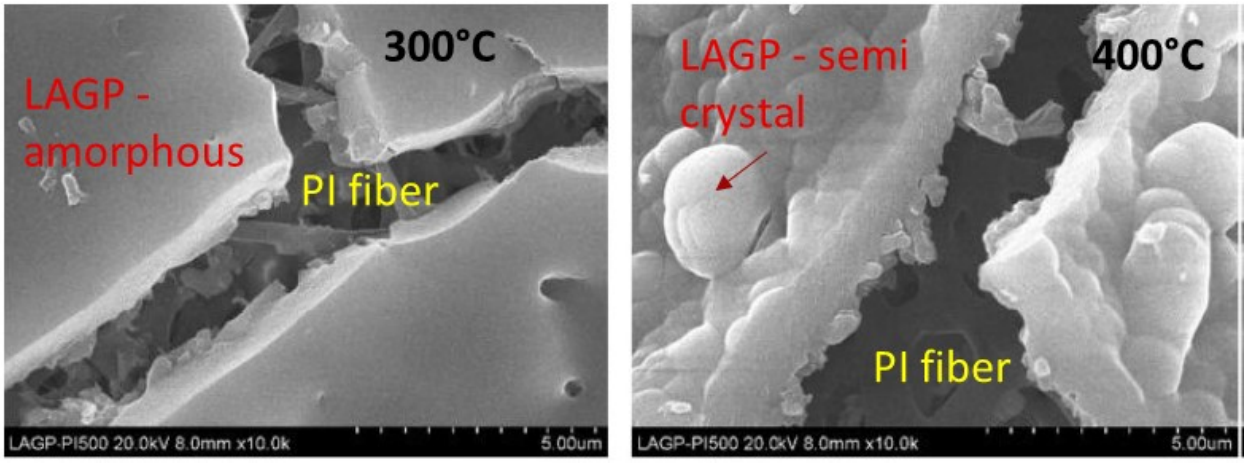

Figure 30. Surface morphology of 500 nm LAGP layer on PI separator partially crystallized at 400°C

The excellent high thermal stabilities of UDRI's thin-film LAGP coating on PI beyond 400°C can prove vital in designing a thermal runaway resistant Li-ion battery. However, there electrical and electrochemical performances must be understood before this technology can be implemented in Li-ion battery technology. Figure 31 shows improved electrolyte uptake as LAGP thickness on PI increases. Good electrolyte uptake capability of the separator will improve cell durability. Noticeably, electrolyte uptake of PI is higher when compared to the commonly used PE separator, as PI has more pores and different surface characteristics/chemistry conducive for absorbing more liquid electrolyte. LAGP coating further improves electrolyte uptake of PI separator.

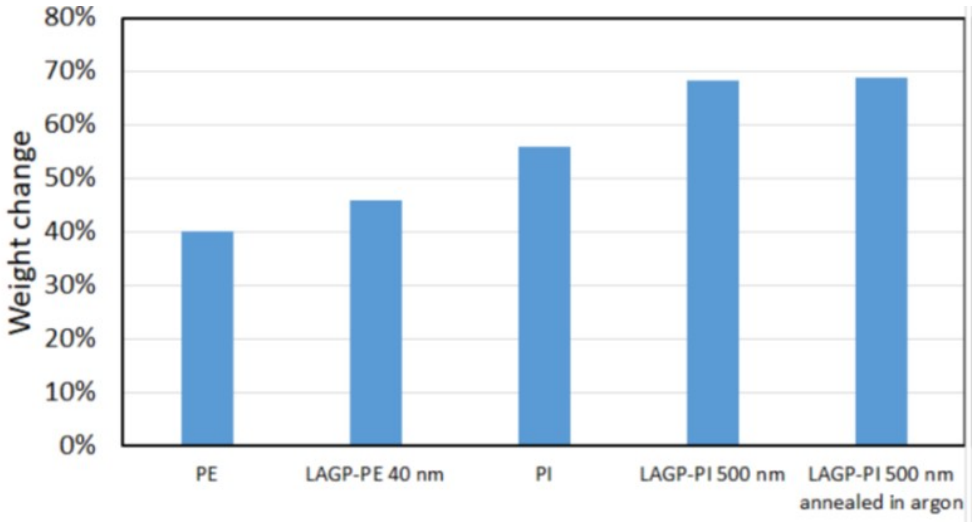

Figure 31. Electrolyte uptake of commercial and UDRI's LAGP-coated separators

Figure 32 shows that as LAGP thickness increases the resistance of liquid electrolyte (1 M $LiPF_6$ in EC/EMC/DMC and 1 wt% VC) soaked PI separators slightly increases. A slight increase in resistance may be due to blocking of some Li^+ transport channels by LAGP, as LAGP deposited by EB-PVD are amorphous (Li^+ insulating) without annealing. As expected LAGP/PI annealed at 350°C shows slightly lower impedance compared to PI, confirming that annealing does make LAGP more Li^+ conducting (Figure 33). Electrical performance can be further improved with optimization of annealing (crystallization) of UDRI's LAGP/PI separator.

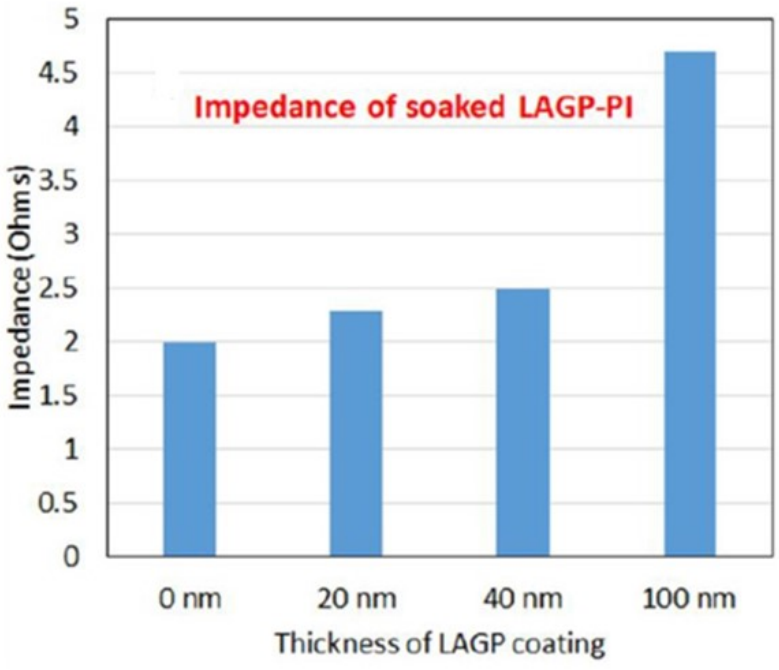

Figure 32. Resistance of PI and LAGP-coated PI separators soaked in liquid electrolyte

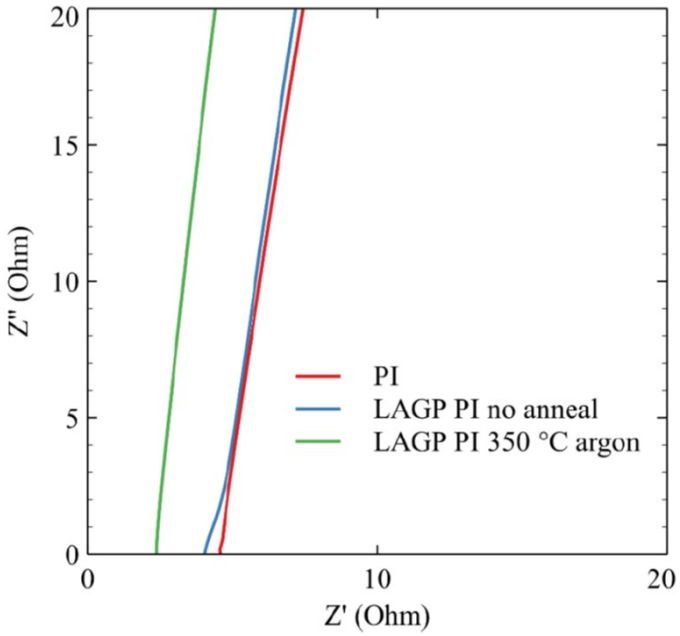

Figure 33. Impedance of liquid electrolyte soaked PI and LAGP/PI separators (with and without LAGP crystallization)

Figure 34 shows the long term cycling performance of UDRI's LAGP-coated PI when compared to the widely used PE commercial separator. A Li-ion cell with PE separator shows slightly better cell capacity but with a higher rate of capacity fade. Additionally, the LAGP/PI shows very stable capacity delivered over a long period of time. This highlights the usefulness of thin-film LAGP coating in providing a durable and consistent Li-ion cell performance.

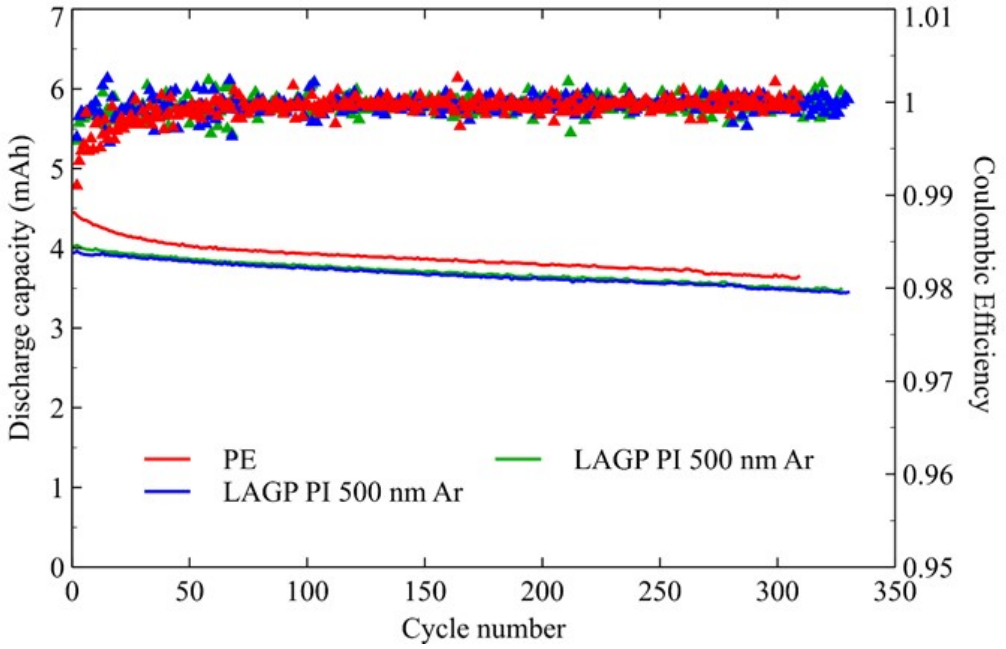

Figure 34. Long-term cycling of Li-ion cells with commercial PE and UDRI's LAGP/PI

Since PI separator shows excellent thermal stability and provides a durable cell cycling performance, we decided to check whether the PI separator is capable of stopping dendrite growth or not. For this test, a Li-ion cell with Li anode was selected, as Li dendrites grow faster with Li metal anode compared to traditionally used graphite anode. The result was very surprising. Several cells cannot be charged even at moderate current densities of < 1 mA/cm^2, suggesting that Li dendrites may have shorted the cell. After opening the cell, we observed some black spots on the separator. SEM characterization revealed Li dendrites features (see Figure 35). Easy dendrite growth observed with the use of the PI separator is due to the large pore size of separator and less tortuous pore distribution in PI compared to PE.

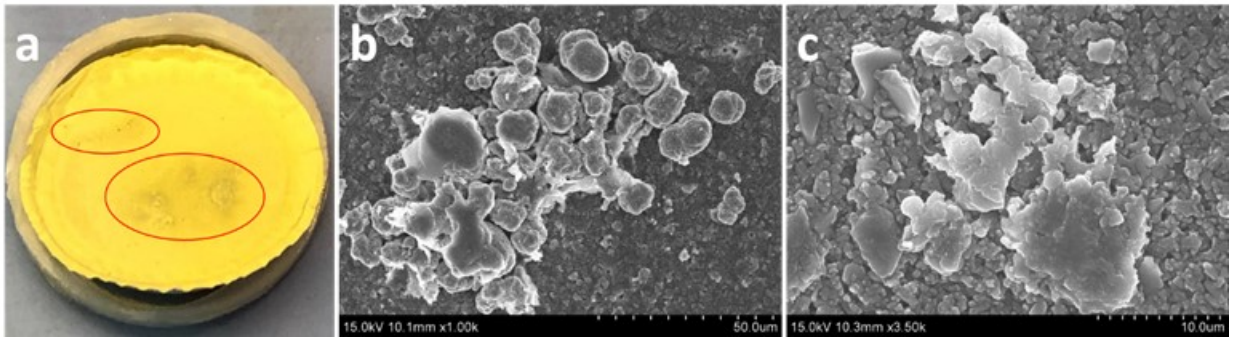

Figure 35. Visual of dendrites on PI separator used in Li-ion cell using Li metal anode

Results in Figure 34 and Figure 35 suggest that PI separator is good for thermally stable performance in traditional Li-ion batteries, but may not be safe in terms of dendrite prevention. This may discourage use of PI in safety-sensitive applications like aircraft. However, these results give us an opportunity to determine if LAGP coating can improve dendrite resistance in PI separator, thus gaining improved thermal stability and resistance to dendrite growth.

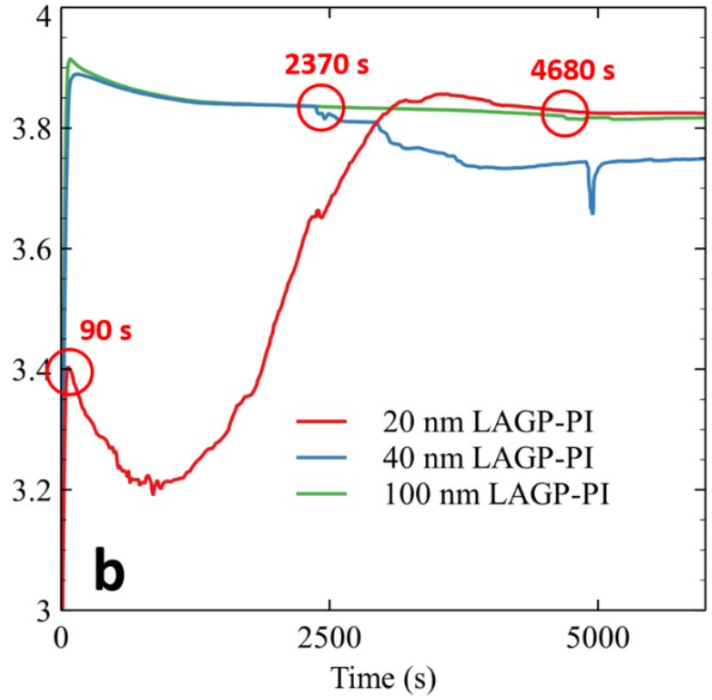

Figure 36. Improved dendrite prevention by UDRI's LAGP/PI

Figure 36 shows Li-ion cell (using Li metal anode) charging with increased LAGP thickness on PI. As noted earlier, Li-ion cell using Li anode and bare PI separator was never chargeable, but with 20 nm LAGP coating cell could charge for 90 sec. As we increased LAGP thickness to 40 nm, charge time increased to 2,370 sec, and with 100 nm LAGP coating, the cell shows dendrite growth symptom delayed to 4,680 sec. These are very encouraging results that demonstrate *LAGP indeed shows better dendrite resistance*. More detailed work needs to be done to advance this finding.

2.1.5 Identified problem and adopted solutions

To ensure the reproducibility of data presented in sections 2.1.1 to 2.1.4 and draw a firm conclusion between LAGP-coated separator versus bare PE or PI, or Al_2O3 (slurry coated) commercial separators, UDRI has investigated many factors during cell development that can affect cell performances. For example, cell performance can be affected by electrolyte impurity,

storage conditions of separators, and cell fabrication environment. These external factors could cause variability in cycling performance of full cells even for the control group (PE separators) from batch to batch, and this variability could largely mask any small effect resulting from separator differences. In addition, the number of reproducible cells fabricated and tested to confirm a particular finding also matters, and so repeat experiments must be done to verify that the separator changes are effective. As good practice, to ensure reproducible results, other researchers further pursuing the work in this report should consider the following:

i) Purchase of same electrolytes and electrode materials from different vendors
ii) Standardization of cell components (check the purity, moisture content, drying, etc.) before cell fabrication
iii) Fabrication of same chemistry cells using glove box in different laboratories, including using a private battery fabrication facility outside UDRI
iv) Purchase of extra battery cycler to test multiple cells for the same tests
v) Post cell test characterizations of cell components of good and bad performing cells
vi) Fabrication of cells by multiple researchers to check human error.

2.1.6 Future outlook

One important factor that was not part of this study was testing of UDRI's LAGP or LLZO-coated separators in a large format Li-ion cells (1 or 2 Ah / cell). All the tests were done at coin cell level (4-5 mAh / cell). Data on UDRI's separator in large format Li-ion can shed extra light on the different advantages and disadvantages (beyond cost) for LAGP, LLZO, and Al_2O_3 ceramic coating by physical vapor deposition techniques (EB-PVD and Sputtering). Further, more work needs to be done on determining the effects of LAGP, LLZO, and Al_2O_3 coating on low and high temperature Li-ion cell performances using more thermal stable electrolytes compared to the commonly used liquid electrolyte. Last but not least, the use of thermally stable electrodes such as ceramic-coated cathode, which is becoming more common as of the writing of this report in 2020 (vs. the start of this effort in 2017), and must be tested with UDRI's coated separators.

2.2 Dendrite sensing technique

Even in normal operation, a Li-ion cell can develop dendrites (a thin metal wire) at one electrode (mostly at anode) that can pierce through the porous separator, connect to another electrode (cathode), and electrically short the cell [5]. The dendrite growth can be aggravated in case of BMS malfunction that can lead to overcharge/deep discharge, or operation of the battery in harsh conditions like sub-zero temperature. In any case, cell shorting due to dendrites can lead to a

sudden cell temperature rise that can cause separator melting followed by degradation of Solid Electrolyte Interphase (SEI), electrodes, and electrolyte, and eventual battery fire as the thermal runaway progresses [1]. This dendrite formation and potential thermal runaway safety issue can be mitigated by developing dendrite-proof cell components, but this has proven to be an elusive goal to date due to fundamental issues with Li electrochemistry and existing battery materials. A more efficient and easy way can be to develop a technique that can detect dendrite growth in their early growth stage before dendrite connects two electrodes electrically, thus allowing the battery to be safely shut down and pulled from service before the short circuit can occur.

During this project, UDRI has developed a unique technique in which a metal layer (metal such as Au or Ag that can be stable in battery electrolyte) can be applied to one side of a separator to detect dendrites in their early stage by monitoring cell voltage between different electrodes and metal (dendrite sensing) layer. For example, as shown in Figure 37, an Au layer can be applied to one side of a separator and placed on anode (the side of separator touching anode will not have Au layer). Subsequently, an extra separator (say PI or PE) without metal layer can be placed between the cathode and metal layer of first separator. This cell design will provide three voltage measurement points: i) voltage between cathode and anode, ii) voltage between reference (Au layer) and cathode, and iii) voltage between reference electrode and anode. For example, if the dendrite grows from the anode toward the cathode, dendrite will reach the reference metal electrode before moving to the second separator. The moment the dendrite reaches from the anode to the reference electrode, the voltage between reference electrode and anode will be zero, and this change in voltage will be the signal to be detected by the BMS. Once the BMS has detected this signal, the BMS can shut down the cell before the dendrite reaches to the cathode, thus preventing cell shorting and subsequent thermal runaway.

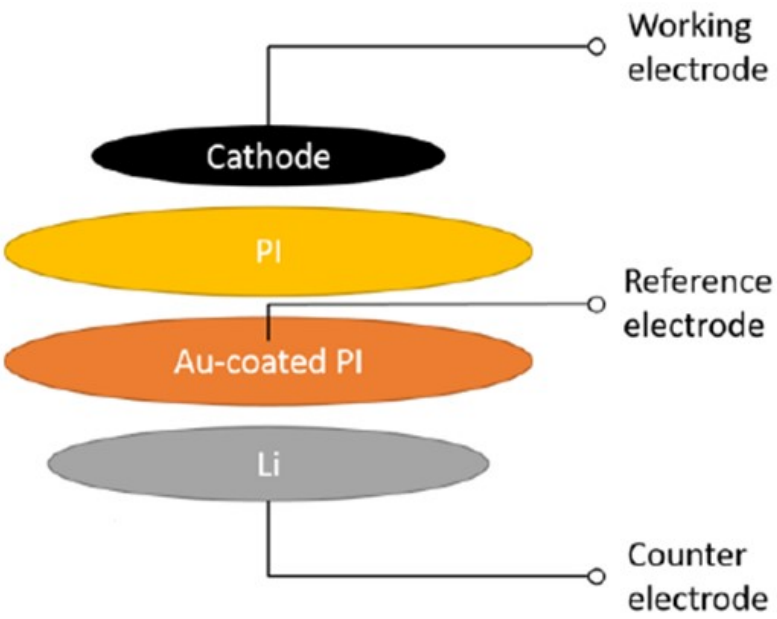

Figure 37. Dendrite sensing design

The early dendrite growth sensing capability within the Li-ion cell, as shown in Figure 37, was carefully designed and tested. As a first step, an optimum thickness of Ag was applied on separator (using magnetron sputtering technique) to achieve electron percolation (see Figure 38). A 30 nm Ag layer provides good electron conduction across the separator surface.

Figure 38. PE coated with different thickness of Ag (from left to right – pristine PE, 6 nm, 12 nm, 18 nm, 24 nm, and 30 nm Ag on PE) for dendrite sensing

Figure 39 shows continuous Ag coating on separator fibers without blocking the separator pores.

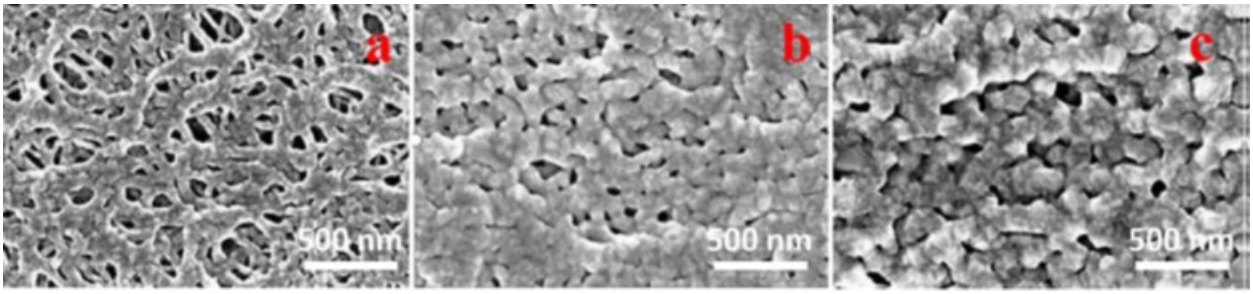

Figure 39. SEM images of Entek separator coated with (a) 6 nm, (b) 18 nm, (c) 30 nm Ag

For good electrochemical performance, the pores of the separator should not be blocked by the metal dendrite sensing layer, as pores provide Li^+ transport channel. Impedance of separators with different Ag layers (6 nm to 30 nm) and soaked in Li-ion liquid electrolyte confirms that there is only a slight increase in resistance for the 30 nm Ag layer (Figure 40).

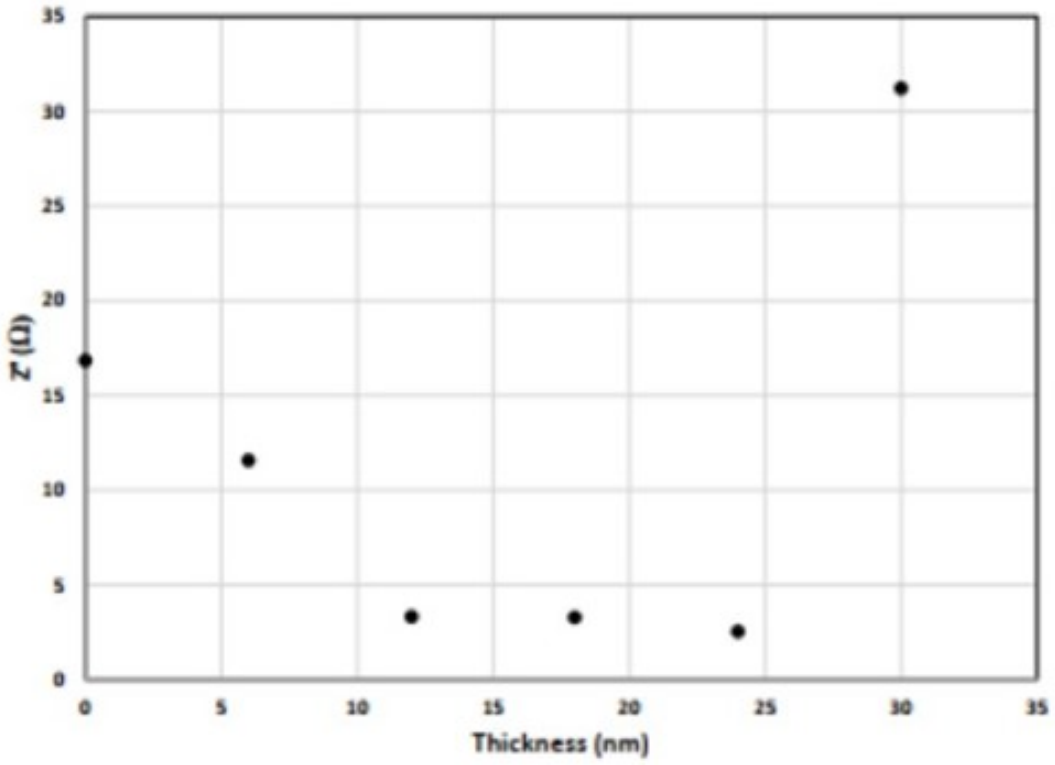

Figure 40. Resistance of liquid electrolyte soaked Ag-coated separators

Figure 41 confirms that the Ag layer deposited using sputtering adheres to the separator surface well, as surface resistance does not change with folding or crushing of separator. Figure 41b confirms that Ag-coated separator is still electron insulating across the thickness of separator, as desired for cell functioning.

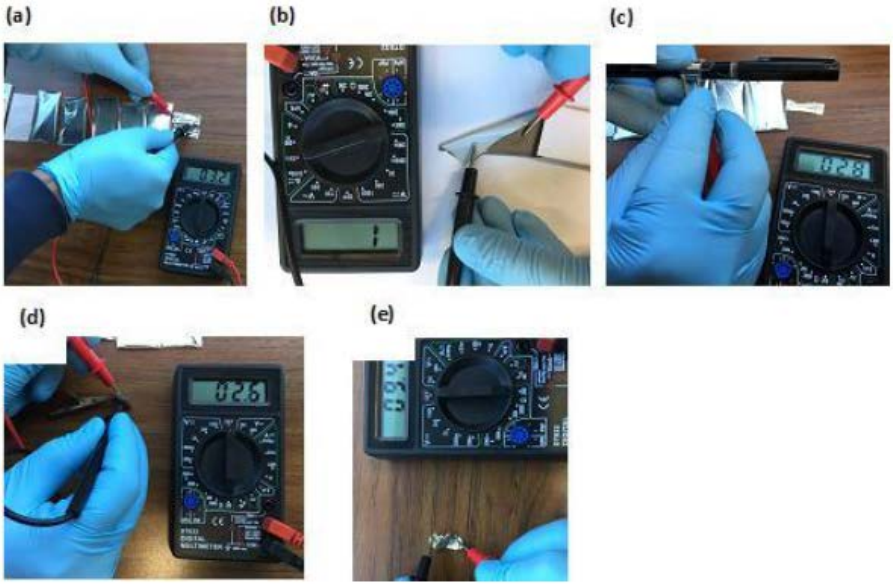

Figure 41. Surface resistances of 30 nm Ag-coated separator: (a) unperturbed, (b) opposite sides of the Ag-coated separator, (c) bending, (d) folding, and (e) crushing

However, the 30 nm Ag layer significantly impacted (20% less capacity) the electrochemical performance of the Li cell (Figure 42), which is undesirable. The poor capacity and fast capacity fade may be attributed to poor stability of Ag with electrolyte or Ag dissolution in electrolyte. Due to this reason, we replaced Ag with Au. Au is a stable/inert material, despite the higher cost, and should resist changes from exposure to the electrolyte.

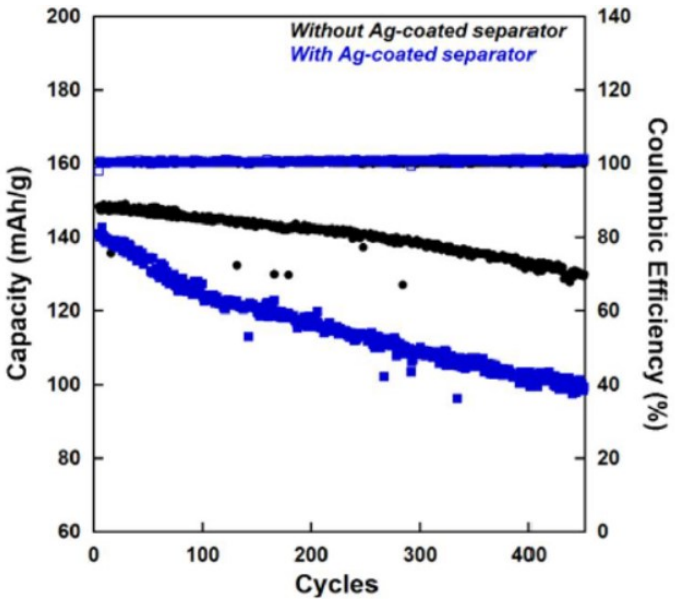

Figure 42. Li-ion cell cycling with and without Ag layer on PE separator

Table 1 shows the surface resistance of Au layer deposited on the PI at four thicknesses, 0 nm (Sample 1), 10 nm (Sample 2), 20 nm (Sample 3), and 30 nm (Sample 4). A 30 nm gold (sample 4) provides good surface electron conduction and will be used for dendrite sensing experiments as described in the following sections (2.2.1 and 2.2.2).

Table 1. Surface resistance [Ω] of Au-coated PI separators

Measurement Distance [cm]	**1**	**2**	**3**	**4**	**5**
Sample 2	223	281	320	351	475
Sample 3	42.7	55.3	58	73.7	83.6
Sample 4	13.2	15.4	17.5	23	25.7

2.2.1 Lithium dendrite sensing

Although graphite anodes are used in commercial Li-ion cells, the occurrence of Li dendrite growth from graphite is extremely rare under normal operation condition. This prevents us from reliably creating conditions for dendrite growth and penetration through separator to test the dendrite-sensing layer. *Therefore, we used Li metal anode to induce easy growth of lithium dendrite*. However, it is unclear what the 'abuse' condition for Li dendrite penetration would be. To answer the question, we started with testing two electrodes nickel manganese cobalt oxide (NMC)/Li cells at extremely high current densities (16 mA/cm^2, 4C rate) (Figure 43). Normally

lithium ion cell works best with ~0.5C rate. Figure 43, shows no sign of dendrite penetration through PE separator at this rate.

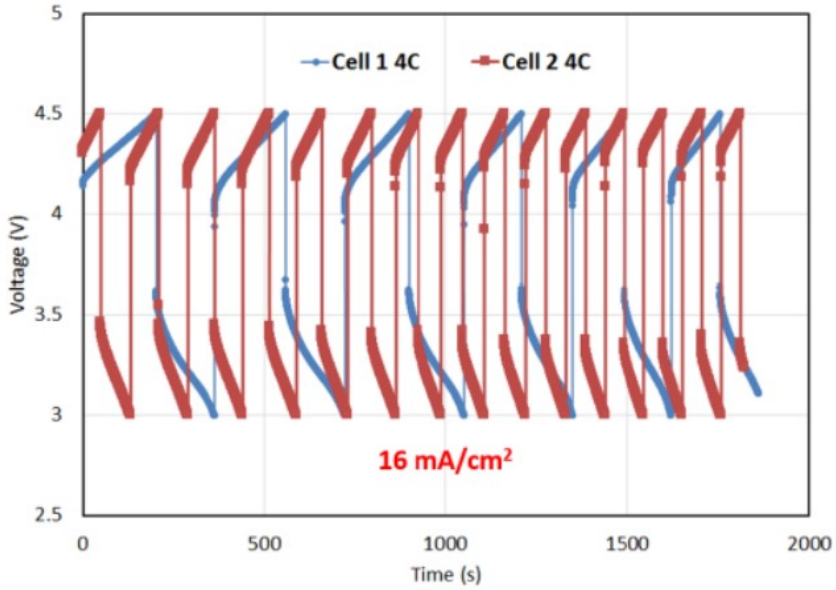

Figure 43. Charge/discharge profile of high loading (4 mAh/cm^2) NMC/Li cells cycled at 16 mA/cm^2

As indicated in Figure 43, Li dendrite penetration through the PE is extremely difficult even at extremely high current density. In order to exert harsher conditions to induce Li dendrite, we applied unidirectional charging to Li-PE-Li cells. The advantage of this configuration is that the charge capacity is not limited by the voltage cut-off of cathodes. The charge current density was 4 mA/cm^2, which should be high enough to induce dendrite penetration according to some literature [5]. Both cells were conditioned at 0.1 mA/cm^2 for 3 cycles prior to the exhaustive charging.

As seen in Figure 44, both cells (a & b) showed stable voltage for the majority of the charge. Eventually, cell voltage increased very sharply until a sudden drop occurred indicating, the cell had been shorted. Based on the current density and the amount of lithium available at the cathode, the timing of the sharp voltage increase largely coincides with capacity needed to exhaust Li. This was confirmed by our observation that no Li was left on the cathode side while a thick porous Li layer was built up on the anode side after the cell was opened. Li exhaustion also explains the sharp voltage increase. Li stripping in carbonate electrolyte is known to be un-uniform, i.e., Li in some regions may be completed stripped before others [13]. The process decreases effective surface area and increases local current density. In the region of high voltage

polarization, the local current density should be much higher than the nominal 4 mA/cm^2, eventually reaching the critical value for dendrite penetration.

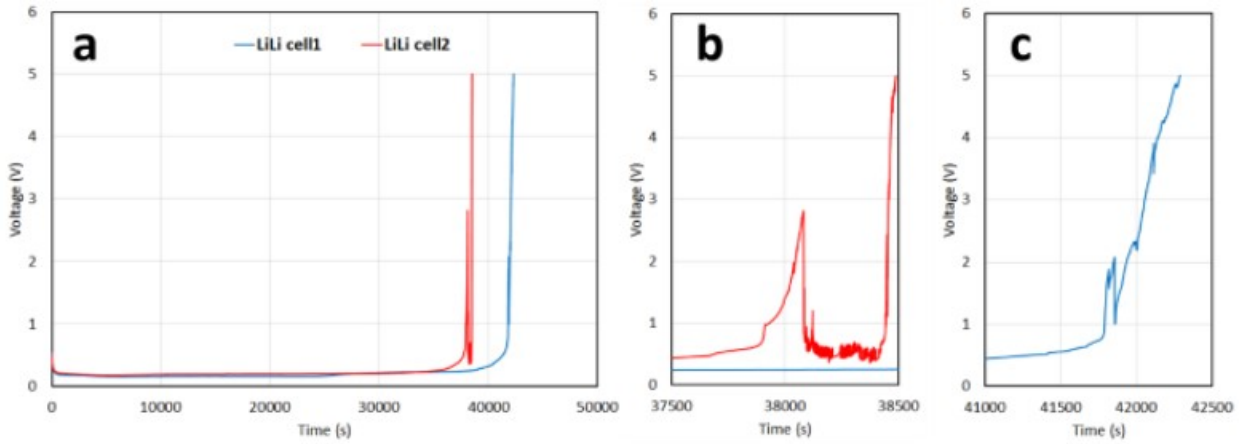

Figure 44. (a) Voltage profile of Li-PE-Li cells under unidirectional charge condition. (b & c) Zoomed in regions of sharp voltage increase and drop

Figure 45 shows sign of early warning of dendrite penetration in a Li/PE/Li cell. This is a three-electrode cell design, as proposed in Figure 37, where one Li plays the role of cathode and another plays the role of the anode. The charge protocol was the same as the two-electrode cells (Figure 44). Voltage between the reference electrode and the anode was monitored, since Li dendrites grow from anode to cathode. The cell voltage (Figure 45) behaves similarly to the two-electrode Li/PE/Li cells (Figure 44). Again, dendrite penetration condition was met only when Li on the cathode was nearly exhausted and the cell voltage sharply increased. Meanwhile, the Au reference electrode displays a stable voltage of 3 V against the anode, typical of Au-to-Li potential. At 62,165 s, the voltage between reference electrode and anode abruptly dropped, signaling that dendrites reached the dendrite-sensing layer. At 62,190 s, a sharp drop of cathode-to-anode voltage signaled that dendrites reached the cathode. There was a time window of about 25 s between the two events, confirming that *the Au dendrite-sensing layer can provide early warnings of internal shorting due to Li dendrites*.

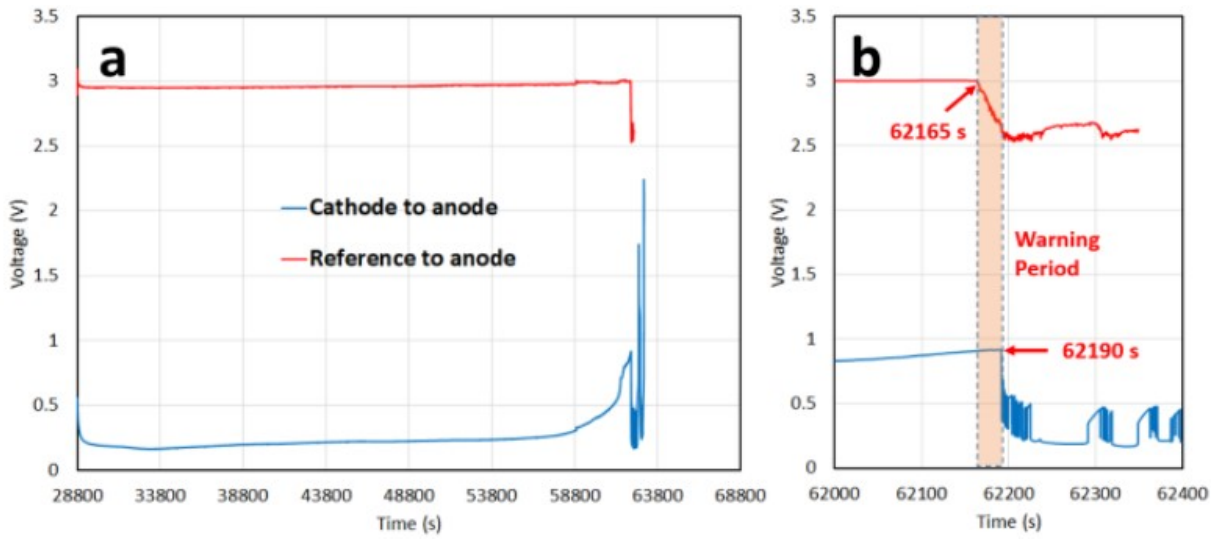

Figure 45. A 25-second early dendrite growth warning

Figure 46 shows a design to detect early dendrite growth in a Li-ion cell with NMC cathode, PI separator, 1M $LiPF_6$ in EC/EMC/DMC electrolyte, and Li anode. The dendrite-sensing layer (Au) is built on one side of a PI separator. At around 4,500 s, both voltages showed a sharp decrease. The blow-up view of the region is shown in Figure 46C. Since we use a data recording protocol of every 300 s or every 5 mV of change, a data-recording event less than 300 s after the previous data collection suggests that the voltage has changed by more than 5 mV; lack thereof indicates the voltage change was less than 5 mV. Therefore, the data collection of cathode-to-anode voltage at 4,554 s indicates a sudden voltage drop of 245 mV from the previous data point 240 s earlier, indicating dendrite penetration from anode to cathode. In the reference-to-anode curve, data collection became increasingly frequent approaching 4,554 s, indicating dendrite penetration from anode to reference. A zoomed-in view of the early warning period shows that at 4,529 s, the voltage dropped by about 20 mV instantly. We believe that this voltage drop is a significant enough anomaly to be picked up by an appropriate battery management system (BMS). The prior smooth drop in voltage indicates soft shorting, which may not be significant enough from a signal processing perspective. Importantly, the early warning provided by the dendrite-sensing layer was about 25 s prior to the complete cell shorting. This result is consistent with our previous experiment using PE separators.

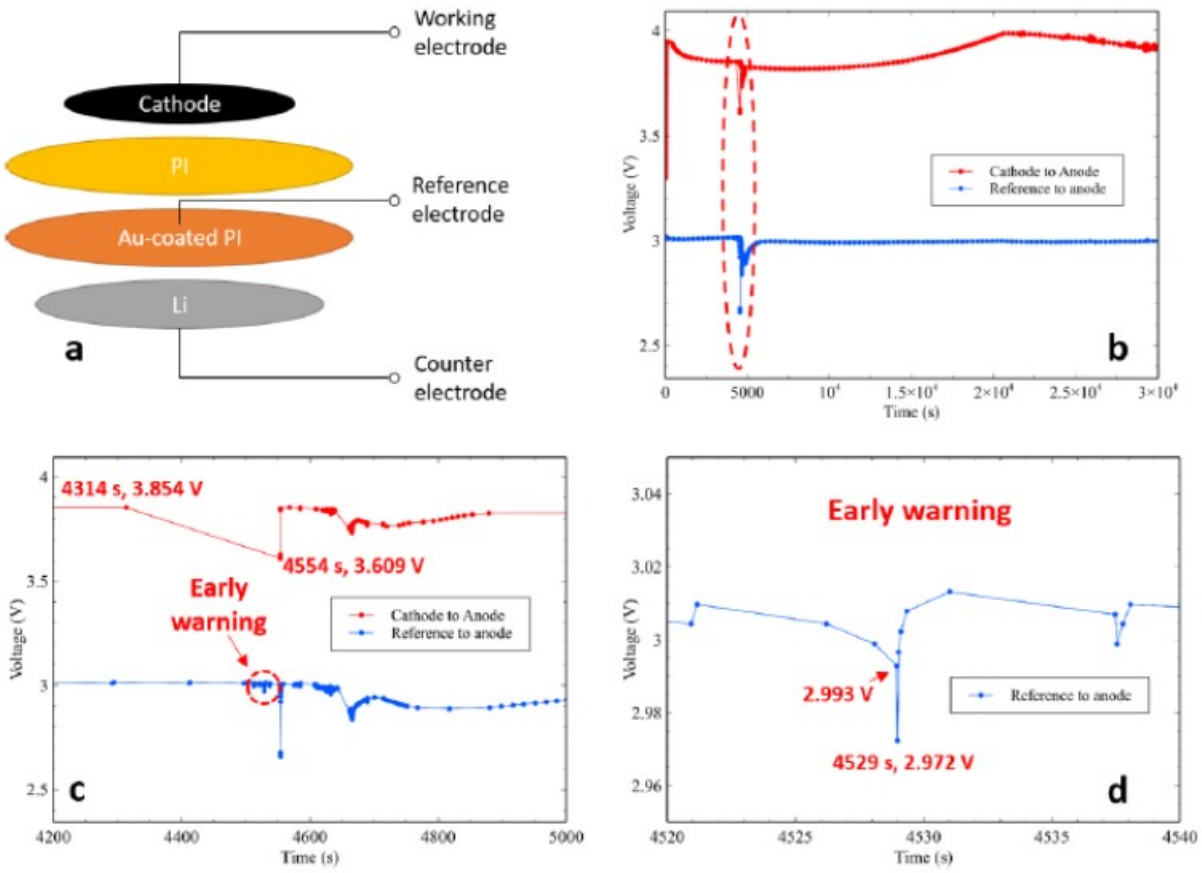

Figure 46. Configuration of the three-electrode cell. b) Voltage profile during the initial 30,000 s of the cell charging. c) Zoom-in of the circled section in b). d) Zoom-in of the circled section in c.

2.2.2 Copper dendrite sensing

Another mechanism of electrochemically induced internal shorting can be through Cu dendrite penetration of the separator when cells are over-discharged [14]. This condition can be met when many cells are connected in series and there has been limited research on the topic. In a Li-ion cell, if the cell voltage is forced below the voltage difference of fully lithiated cathode and fully delithiated graphite anode, Cu from the anode current collector can dissolve electrochemically and deposit on the cathode, often in the form of dendrites. *Note that Cu is much harder (mechanically) than Li, so Cu dendrites are much more destructive to separators than Li dendrite*. We, therefore, attempted to create internal shorting through Cu dendrite and to detect Cu dendrite growth using an Au layer deposited on the separator (PE), as shown in Figure 47.

As shown in Figure 47, the voltage from cathode to reference was monitored instead because Cu dendrites grow from cathode to anode, in contrast to Li dendrites, which grow from anode to cathode. Figure 47B shows the voltage profile of the entire test sequence, which consists of an

initial rest of 10 h, three charge/discharge cycles at C/5, a constant voltage period at 3 V, an over-discharge period at constant current of 0.2 mA for 10 h, another rest period, and a charge period. Before the over-discharge period, the cathode-to-anode and the cathode-reference voltages were smooth at expected values. As discussed earlier, the over-discharge voltage profile features an initial smooth decrease, and inflection point and a slow rising period. The point at the lowest voltage marks the onset of Cu dissolution/deposition. Again, there was no clear signal of dendrite penetration from the cathode-to-anode voltage, but the cathode-to-reference voltage dropped sharply at 252,400 s (Figure 47C & Figure 47D), indicating that Cu dendrites had reached the reference electrode/dendrite-sensing layer. Close inspection shows that the cathode-to-anode voltage changed by only 5 mV in 10 s while the cathode-to-reference voltage decreased by 360 mV. This anomaly should be easily detected by BMS, which provides about 10 s of early warning. The 25 s early warning with Li dendrite and 10 s early warning with Cu dendrite may be due to the fact that Cu is harder than Li dendrite and are more effective in cell shorting. These are early results and conclusions need to be verified further with future work.

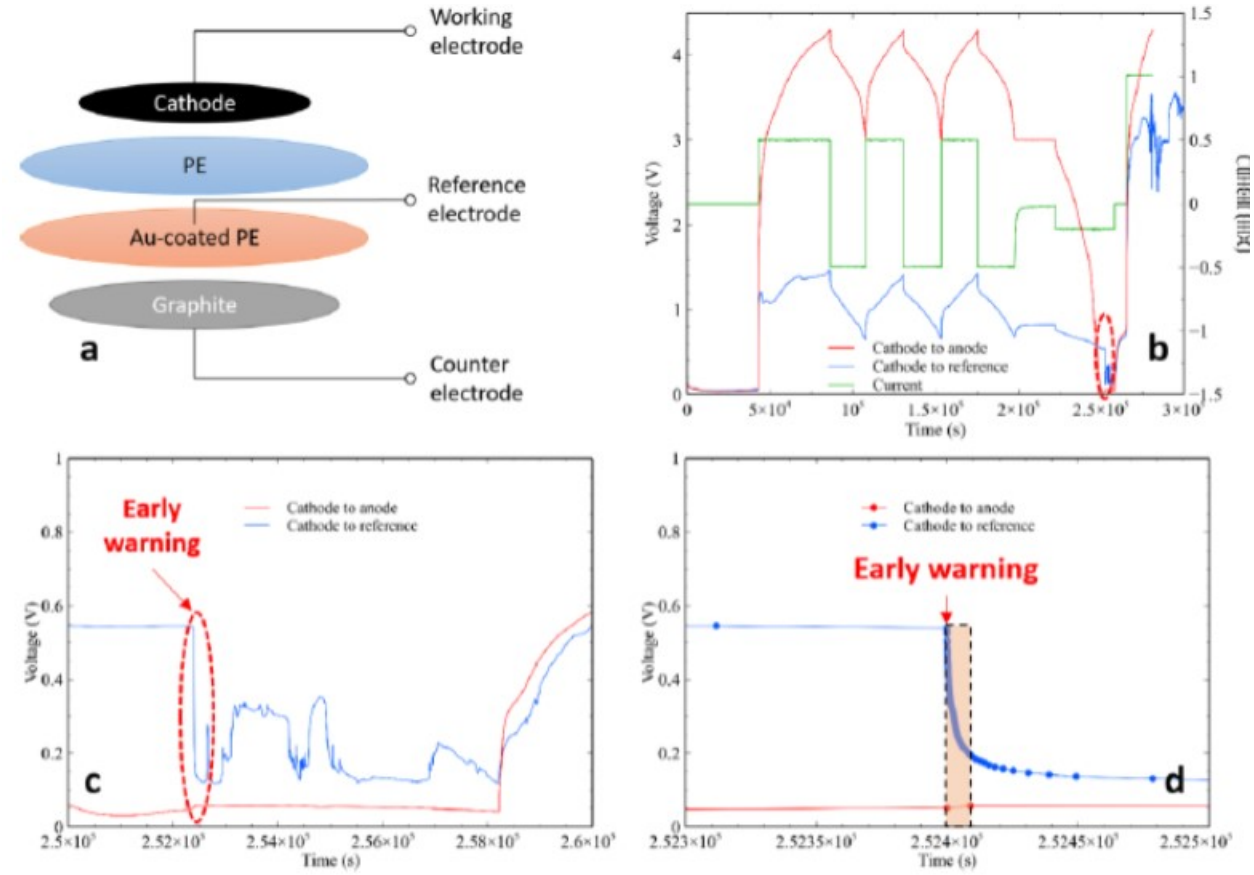

Figure 47. Early detection of Cu dendrites

2.2.3 Identified problem and adopted solutions

Figure 45 through Figure 47 showed the possibility of detecting dendrites at their early growth period, but this method of inducing Li dendrite penetration was highly uncontrollable and not very reproducible. It is not clear what the critical current density was. Without a predictable mode of failure, it is difficult to compare the dendrite suppression characteristics of different separators. Therefore, we need to do more work to determine if ceramic coatings reduce dendrite growth. Moreover, once predictable dendrite generation and growth conditions are known, other techniques, such as dendrite sensing via ultrasonic waves and measurement of differential temperature with and without dendrite cell shorting, would make for good future research targets. Otherwise, the voltage detection from the Li or Cu dendrite formation suggests that other researchers should consider studying this voltage effect to determine if this is universal, or unique to the batteries we studied. If a universal phenomenon, BMS units could be programmed to detect this voltage event, which would in turn improve battery safety.

2.2.4 Future outlook

The dendrite sensing technology demonstrated by UDRI clearly shows the technology's ability to detect the formation of metal dendrites and provide a sufficient detection window before a full dendrite-shorting event occurs. Therefore, the sensing technology can be used in conjunction with a battery management system (BMS) to stop the operation of the cell before thermal runaway can occur.

With any sensing technology, an essential set of questions to answer is the impact of signal to noise on the sensing technique. The triggering signal for dendrite detection is an instantaneous change in voltage at the sensing terminal. Similarly, a voltage change occurs with a change in current due to cell polarization. An associated algorithm must be developed to determine when a triggering signal is a result of a dendrite versus a change in cell polarization to implement the dendrite-sensing layer into a practical battery system. The developed algorithm will likely be reliant on dI/dt and dV/dt values to assess when a significant change in voltage is not attributed to a change in current and, therefore, the formation of a dendrite.

To develop the requisite algorithm, future research would need to produce a suite of several cells, with the sensing layer, that is capable of demonstrating consistent behavior. These cells would need to be tested under various dynamic current conditions, collecting a reliable set of test data capable of separating dynamic behavior vs. dendrite-induced behavior. The acquired test data would then need to be tested via several optimized control algorithm families, including but not limited to Artificial Neural Networks and Fuzzy Logic Control.

3 Conclusions

The project successfully demonstrated that a thin-film (20-500 nm), binder-free ceramic coating of commercial separators can significantly improve the thermal stability of separator desirable to improve battery safety. This can be achieved with commercial ceramics as well as next generation ceramics, provided the right type of ceramic deposition methodology is used. To gain a better balance of battery properties in the ceramic-coated separator, higher temperature polymer separators (such as those made from polyimide) may be needed to allow for ceramic coating separation. However, the trade-space for thermal stability benefit and battery performance is limited, and more research is needed in this area to better optimize ceramic thermal protection/separator electrochemical performance. Still, the use of ceramic coatings on separators provided the right ceramic deposition technique is used, will lower the risk of thermal failure/thermal runaway in Li-ion batteries.

Dendrite formation, which will lead to short circuits and thermal runaway in Li-ion batteries, was successfully detected via the use of a thin metal layer of gold (Au) on the separator to detect both Li and Cu dendrite formation. The dendrites could be detected with discrete voltage events, and their detection can be fed into algorithms for battery management system (BMS) programming, which would further improve Li-ion battery safety.

Combining ceramic-coated separators and the Au coatings for dendrite detection would be an obvious thing to combine in future work, but some research on how to combine these two materials in an effective separator would need to be conducted first. Otherwise, the results of this report have found two technologies that can be implemented in the near future to improve the fire safety of Li-ion batteries used in aircraft, as well as other consumer applications.

4 References

1. X. Feng, M. Ouyang, X. Liu, L. Lu, Y. Xia, X. He, “Thermal runaway mechanism of lithium ion battery for electric vehicles: A review”, Energy Storage Mater. 10 (2018) 246–267.
2. J.Y. Kim, D.Y. Lim, “Surface-modified membrane as a separator for lithium-ion polymer battery”, Energies 3 (2010) 866.
3. J.A. Choi, S.H. Kim, D.W. Kim, “Enhancement of thermal stability and cycling performance in lithium-ion cells through the use of ceramic-coated separators”, J. Power Sources. 195 (2010) 6192.

4. J. Kumar, P. Kichambare, A.K. Rai, R. Bhattacharya, S. Rodrigues, G. Subramanyam, “A high performance ceramic-polymer separator for lithium batteries”, J. Power Sources. 301 (2016) 194.
5. T. Wang, R.V. Salvatierra, J.M. Tour, “Detecting Li dendrites in a two-electrode battery system”, Adv. Mater. 31 (2019).
6. B. Kumar, D. Thomas, J. Kumar, “Space-charge-mediated superionic transport in lithium ion conducting glass-ceramics”, J. Electrochem. Soc. 156 (7) (2002) A506.
7. F. Han, Y. Zhu, X. He, Y. Mo, C. Wang, “Electrochemical Stability of $Li_{10}GeP_2S_{12}$ and $Li_7La_3Zr_2O_{12}$ Solid Electrolytes”, Adv. Energy Mater. 6 (2016) 1501590.
8. N. Kamaya, et. al. “A Lithium Superionic Conductor”, Nature Mater. 10 (2011) 682.
9. K.M. Kim, L.R. Hepowit, J.-C. Kim, Y.-G. Lee, J.M. Ko, “Enhanced separator properties by coating alumina nanoparticles with poly (2-acrylamido-2-methyl-1-propanesulfonic acid) binder for lithium-ion batteries”, *Korean J. Chem. Eng.* 32 (2015) 717.
10. S.R. Baldwin, “A review of state-of-the-art separator materials for advanced lithium-based batteries for future aerospace missions, NASA/TM—2009-215590 (https://ntrs.nasa.gov/archive/nasa/casi.ntrs.nasa.gov/20090017842.pdf).
11. S. Ma, et. al., “Temperature effect and thermal impact in lithium-ion batteries: A review”, Progress in natural science: materials international, 28(6) (2018) 653.
12. M. Li, et.al., “Novel polyimide separator prepared with two porogens for safe lithium-ion batteries”, ACS Appl. Mater. Interfaces 12(3) (2020) 3610.
13. Y. Wang, Q. Li, S. Cartmell, H. Li, S. Mendoza, J.G. Zhang, Z.D. Deng, J. Xiao, “Fundamental understanding and rational design of high energy structural microbatteries”, Nano Energy. 43 (2018) 310.
14. C. Chen, G. He, J. Cai, Z. Zhao, D. Luo, "Investigating the overdischarge failure on copper dendritic phenomenon of lithium ion batteries in portable electronics”, *2019 22nd European Microelectronics and Packaging Conference & Exhibition (EMPC)*, Pisa, Italy, 2019, pp. 1-6, doi: 10.23919/EMPC44848.2019.8951808.

A Materials development and characterizations

Separator selection

Commercially available separators most commonly employed in LIBs include multilayer polymer separators made from polypropylene (PP) and PE. They are usually manufactured via a "wet" or "dry" process. In the "dry" process, PP and/or PE is/are extruded into a thin sheet and subjected to rapid drawdown (Celgard). The sheet is then annealed at 10 to 25 °C below the polymer melting point to control the crystallite size and orientation. Next, the sheet is rapidly stretched in the machine direction to achieve slit-like pores or voids at 35-45% porosity (see Figure 48). On the other hand, polyolefin separators based upon ultra-high molecular weight PE are usually produced in a "wet" or "gel" process involving extrusion of a plasticizer/polymer mixture at elevated temperature, followed by phase separation, biaxial stretching, and extraction of the pore former (i.e., plasticizer). The resultant separators have elliptical or spherical pores and porosity in the 40-50% range (Figure 48). Because of the biaxial orientation, good mechanical properties are achieved in both the machine and transverse directions. The separators also have strong chemical and abrasion resistance, and good wettability with organic solvents, due to which, PE separators have found wide use in LIBs. Therefore, we selected the polymer separator (PE) fabricated using the wet process (Entek) due to its spherical and elliptical pores in the biaxial direction, which results in higher mechanical stability and good electrolyte wettability for depositing ceramics and metals.

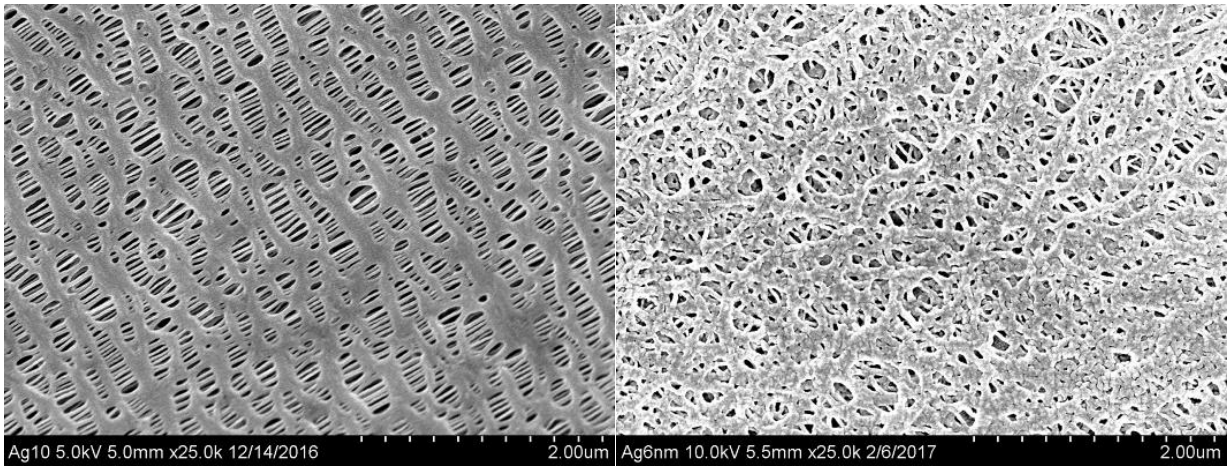

Figure 48. SEM images showing commercial polymer separators fabricated using an (a) dry and (b) wet process

Coating Methods

Entek separators were used as substrates for depositing ceramic layers on each side of the separator. The Electron Beam Physical Vapor Deposition (EB-PVD) technique for thin-film depositions is a scalable, fast, and cost-effective technique. The EB-PVD system which employs an electron beam (EB) source was used to evaporate ceramic layers at a high rate (≈ 2 nm/sec.) on a large surface area (> 30 cm^2) of the Entek separator. A chunk of ceramic sample was placed in a graphite crucible as the target [4]. Entek separators served as substrates for thin-film ceramic deposition and were mounted on a metal plate. The chamber was evacuated to a base pressure of < 10^{-6} Torr. The deposition rate was controlled by the power of the EB and the distance between the crucible and substrate. During EB-PVD, coating material thus undergoes significant phase change (solid to gas). For example, we start with crystalized LAGP (Li^+ conducting phase), but LAGP deposited by EB-PVD becomes amorphous (less or no Li^+ conducting), which requires post-deposition conditioning (crystallization). Magnetron sputtering, in which the deposition material is ionized in a neutral gas, is expected to deposit LAGP with better crystallinity, and hence better Li^+ conduction even without the need of post-fabrication conditioning. Pulsed laser deposition (PLD), on the other hand, is also a PVD technique, where instead of an electron beam, a high-power laser is used to strike the source material, which is then vaporized and deposited on the target (separator). A major difference between EB-PVD and PLD is that high deposition rates are possible at relatively low substrate temperatures with very high material utilization efficiency in EB-PVD. Nevertheless, the morphologies of the deposited film are different leading to different properties.

Ceramic Selection

Lithium superionic conductor (LiSICON) based ceramic solid electrolytes, such as LAGP (σ = 5 x 10^{-3} S/cm at 23 ºC) [6], affords many other favorable properties. Their advantages include their solid-state nature, broad electrochemical window (> 5 V), negligible porosity (preventing Li dendrite propagation and active material diffusion), high mechanical stability against Li dendrite penetration, and single ion conduction (high Li^+ transference number), enabling high energy density battery chemistries, and mitigating safety and packaging issues associated with conventional Li batteries.

Despite the good mechanical property and high ionic conductivity, LAGP shows poor processing, device integration, and anode instability. It is likely that a single ceramic electrolyte system is unable to fulfill all the desired electrolyte characteristics. While we continue to optimize LAGP coating separators, we explore the use of two other known Li-ion conductors, $Li_7La_3Zr_2O_{12}$ (LLZO) and $Li_{10}SnP_2S_{12}$ (LSPS) [7,8]. The class of Li garnet electrolytes (e.g.,

$Li_7La_3Zr_2O_{12}$, LLZO) show favorable Li metal compatibility but require high processing temperatures (LAGP ~850 °C; LLZO ~1200 °C). On the other hand, sulfur-based ion conductors such as $Li_{10}SnP_2S_{12}$ (LGPS) have higher Li^+ conductivity (~ 10^{-2} S/cm) [8] than LAGP (10^{-3} to 10^{-4} S/cm). However, one major limitation of LGPS is air-sensitivity, requiring a highly inert environment for processing. The limitation of LLZO is their lower chemical stability against common cathode materials.

Alumina (Al_2O_3) is an inactive ceramic (possessing negligible Li-ion conductivity) with excellent chemical stability and thermal stability [9]. It has been widely used to decorate commercial polymeric separators for stability improvement. We have also investigated PE separators with EB-PVD-deposited Al_2O_3 and compared them with commercial Al_2O_3-coated separators.

Thermal Shrinkage measurement

Discs of pristine PE and solid-electrolyte-coated PE samples were cut and placed between two ceramic tiles in a vacuum oven (MTI Corp.) for heating at ambient pressure.

Thermal shrinkage of battery separators is an important parameter defining the safety of a battery cell. Excessive shrinkage at elevated temperatures may result in cell shorting. In order to determine the thermal properties (i.e. shrinkage) of ceramic-coated separators, we annealed circular pieces of the separators (ca. 17 mm diameter) at different temperatures for two hours. The diameters of the discs were measured with Vernier Calipers before and after annealing conditions to determine the shrinkage percentage of the samples. The annealing was done for two hours in an oven at 1 °C/min heating and cooling rates in air. A fresh separator was used at each temperature.

Surface Morphology

The pristine PE and ceramic-coated separators were first coated with 5 nm gold using a benchtop sputtering device (Anatech USA) prior to SEM imaging. A Hitachi S-4800 at 5 kV accelerating voltage was employed for studying the morphology of the coated separators.

Electrolyte Wettability of Separators

Contact angle measurement (Figure 49) can be used to evaluate the interaction of liquids with surfaces. It quantifies the wetting ability of the solid surface by a liquid and reflects the strength of the molecular interactions between the liquid and solid under specific conditions. PP/PE separators are inherently non-polar which results in poor wettability with polar electrolytes. Poor

wettability with the electrolyte gives rise to high cell impedance due to poor ionic conductivity through the battery separator.

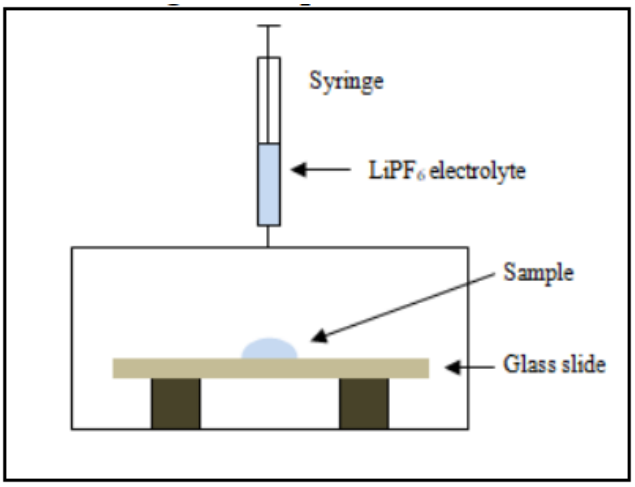

Figure 49. Schematic of contact angle measurement

Microscopic glass slides were cleaned with acetone, dried in the oven (50 °C for 30 min), and used as substrates for mounting separator samples to be tested. The experimental setup (Figure 49) consists of a syringe with a needle whose tip was fixed at a few millimeters above the separator substrates. Consecutive images of the separator were taken (Nikon D-500 DSLR, AF-S Nikkor 85 mm 1:3.5 G ED (micro/macro lens) starting immediately after 30 sec of dropping the electrolyte (1 M $LiPF_6$ in ethylene carbonate (EC): dimethyl carbonate (DMC): ethyl methyl carbonate (EMC) (1:1:1 = v:v:v) with 2 wt% vinylene carbonate (VC) from the syringe. The contact angles were then measured using IMAGE-J.

Electrolyte uptake

Electrolyte uptake is an indicator of the wettability of the separators with certain electrolyte and electrolyte retention. High electrolyte uptake is preferred for good wetting properties. Separators were punched with an 18 mm punch and weighed (W_1). They were then immersed into standard liquid electrolyte for 24 h. The excess electrolyte solution on its surface was removed by letting them dry on the surface of the vials for one hour before measuring the final weights (W_2). The liquid uptake of the separators at different times were measured in a glove box filled with argon according to the following expression:

$$\eta = \frac{W_2 - W_1}{W_1} * 100\%$$

Electrical characterization

Electrochemical impedance spectroscopy (EIS) was employed to understand Li-ion transport of separators soaked in liquid electrolytes. The separators were sandwiched between two pieces of stainless steel electrodes and assembled in CR2032 coin cells. 1 M $LiPF_6$ in EC:EMC:DMC (1:1:1 = v:v:v) + 2 wt% VC electrolyte.

Battery shutdown and breakdown (In-situ impedance testing)

In-situ impedance measurement was employed to further characterize the thermal stability (separator shutdown & breakdown) of separators, a more practical and accurate way of characterization as this involves thermal stability measurement in the presence of electrolyte.

The separator was assembled in a coin cell with stainless steel plates as current collectors. A copious amount of standard electrolyte for full cell testing (1 M $LiPF_6$ in EC/DMC/EMC and 2 wt% VC) was added. The coin cell was assembled using high-temperature gaskets and was sandwiched by a clamp set up to counter the pressure inside the cell, since the test temperature is above the boiling temperature of some electrolyte components. The cell temperature was slowly raised at 1°C/min from 100°C to 190°C in an environmental chamber, while the cell impedance was monitored. Separator impedance as a function of temperature was measured using a multi-frequency impedance analyzer while the separator material (soaked in the liquid electrolyte) was maintained under constant pressure between two stainless steel discs. Figure 50 shows a schematic representation of the separator under test, and its impedance was measured as a function of frequency, and temperature scan rate.

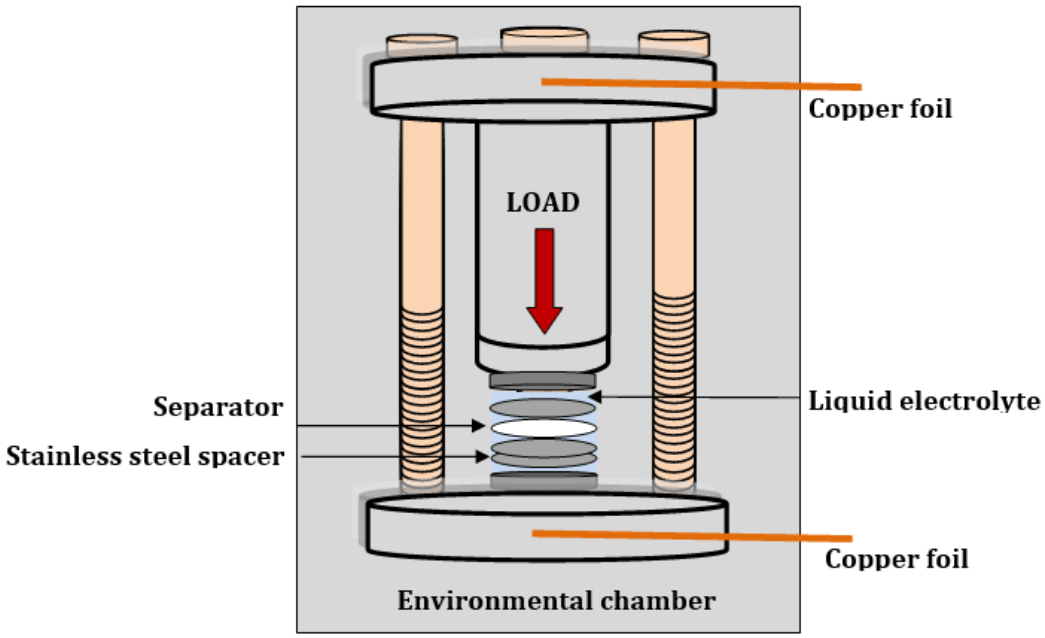

Figure 50. In-situ impedance measurement fixture showing separator/electrolyte layered between stainless steel

Electrode Preparation

Coin cells were made with ($LiNiCoMnO_2$) NMC111 as the positive material and graphite as negative material, and different separators (see Figure 51). The positive electrodes had a mass loading of 22.4 mg/cm^2. The electrode formulation was 94% active material, 3% PVDF binder, and 3% super P carbon black by weight. The graphite negative electrodes had a loading of 12.8 mg/cm^2, corresponding to an N/P ratio of 1.0. The electrode formulation was 96% active material, 2% PVDF binder, and 2% super P carbon black by weight. The obtained NMC111 and graphite slurries were doctor-bladed onto aluminum and copper foils, respectively, and dried at 80 °C for 1h. Before their use, all electrodes were dried under vacuum at 110 °C overnight. For NMC111/graphite full cells, a cathode-to-anode capacity balance ratio of 1.0 was selected considering 150 mAh/g for NMC111 and 300 mAh/g for graphite.

Cell fabrication

As seen in Figure 51, 2,032 coin-type cells with two PE (Entek) separators and the graphite anodes were assembled in an argon-filled glove box. AC impedance data were obtained after formation cycling using a Solartron Impedance analyzer in the 0.1-10^6 Hz frequency range at 22°C. The influence of coated vs non-coated separators on the cycling performance of NMC111/graphite full cells was examined employing 75 µL of a standard electrolyte consisting

of 1 M $LiPF_6$ in (1:1:1 = v:v:v) and 2 wt% VC. All LIB cells were first ‘conditioned’ at room temperature by cycling initially at 0.05 C charge/discharge for 3 cycles, and finally cycled at 0.5 C rate for long-term cycling between 3.0 - 4.3V. These cycle tests are made without extended hold periods at the end of charge.

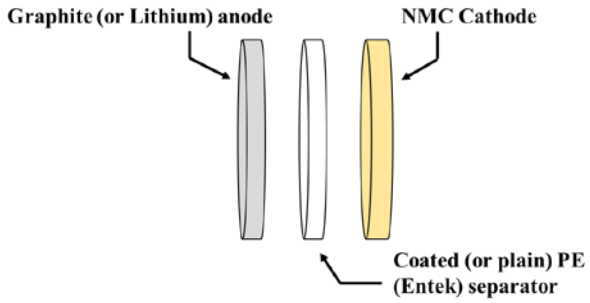

Figure 51. General configuration for testing of the LAGP-PE separators in a Li-ion coin cell